Electronic Supplementary Material (ESI) for Journal of Materials Chemistry C.
This journal is © The Royal Society of Chemistry 2022

ELECTRONIC SUPPLEMENTARY INFORMATION

Slow magnetic relaxation in Nd(III) and Sm(III) complexes formed in three-dimensional lanthanide-dicyanidometallate(I) frameworks exhibiting luminescent properties

Kunal Kumar,[†] Guanping Li,[†] Olaf Stefanczyk,[†] Szymon Chorazy,[‡] Koji Nakabayashi,[†] and Shin-ichi Ohkoshi[,†]*

[†]*Department of Chemistry, School of Science, The University of Tokyo, 7-3-1 Hongo, Bunkyo-ku, Tokyo, 113-0033, Japan.*

[‡]*Faculty of Chemistry, Jagiellonian University, Gronostajowa 2, 30-387 Krakow, Poland.*

*Corresponding author: ohkoshi@chem.s.u-tokyo.ac.jp

The representative asymmetric unit with atoms labelling. (Figure S1) S3

Representative view of the crystal packing of all four compounds along ab plane. (Figure S2) S4

Representative view of the crystal packing of all four compounds along ac plane. (Figure S3) S5

List of Selected bond lengths for **NdAg**, **NdAu**, **SmAg**, and **SmAu**. (Table S1) S5

List of Selected bond angles for **NdAg** and **NdAu**. (Table S2) S6

List of Selected bond angles for **SmAg** and **SmAu**. (Table S3) S7

Results of Continuous Shape Measure (CSM) analysis for **NdAg**, **NdAu**, **SmAg**, and **SmAu** compounds for $[Ln^{III}(H_2O)(CN)_6]^{3-}$-moiety. (Table S4) S8

Experimental powder X-ray diffraction patterns of **NdAg**, **NdAu**, **SmAg**, and **SmAu**. (Figure S4) S9

The infrared spectroscopy (IR) for **NdAg**, **NdAu**, **SmAg**, and **SmAu**. (Figure S5) S9

Thermogravimetric curves of molecular frameworks with Ag(I) ion **NdAg** and **SmAg** (upper part) along with the Au(I) containing compounds **NdAu** and **SmAu**. (Figure S6) S10

Temperature dependent product of temperature with molar magnetic susceptibility (χ_MT) for Nd(III) -having compound (a) and Sm(III) -containing compounds (b) along with field dependence magnetization (*M-H*) data (c and d). (Figure S7) S12

Overlapped frequency dependencies of out–of–plane χ_M" magnetic susceptibility for **NdAg** (a;b) and **NdAu** (d;e) in H_{ac} = 3 Oe at T = 1.85 K for given external *dc* magnetic fields. (Figure S8) S13

Overlapped frequency dependencies of out–of–plane χ_M" magnetic susceptibility for **SmAg** (a;b) and **SmAu** (c;d) in H_{ac} = 3 Oe at T = 1.85 K for given external *dc* magnetic fields. (Figure S9) S14

Ac magnetic properties of the **NdAg**, for H_{dc} = 2000 Oe and H_{ac} = 3 Oe: variation of in–plane, χ_M' (a) frequency components of the compound magnetic susceptibility and the related χ_M"–χ_M' Argand plots (b). (Figure S10) S15

Ac magnetic properties of the **NdAu**, for H_{dc} = 2000 Oe and H_{ac} = 3 Oe: variation of in–plane, χ_M' (a) frequency components of the compound magnetic susceptibility and the related χ_M"–χ_M' Argand plots (b). (Figure S11) S15

Ac magnetic properties of the **SmAg**, for H_{dc} = 3000 Oe and H_{ac} = 3 Oe: variation of in–plane, χ_M' (a) frequency components of the compound magnetic susceptibility and the related χ_M"–χ_M' Argand plots (b). (Figure S12) S16

Ac magnetic properties of the **SmAu**, for H_{dc} = 3000 Oe and H_{ac} = 3 Oe: variation of in–plane, χ_M' (a) frequency components of the compound magnetic susceptibility and the related χ_M"–χ_M' Argand plots (b). (Figure S13) S16

Parameters obtained by fitting the Argand χ_M"–χ_M' plots (H_{dc} = 2000 Oe, Figure S10) of **NdAg** using the generalized Debye model for single relaxation process. (Table S5) S17

Parameters obtained by fitting the Argand χ_M"–χ_M' plots (H_{dc} = 2000 Oe, Figure S11) of **NdAu** using the generalized Debye model for single relaxation process. (Table S6) S17

Parameters obtained by fitting the Argand χ_M"–χ_M' plots (H_{dc} = 3000 Oe, Figure S10) of **SmAg** using the generalized Debye model for single relaxation process. (Table S7) S18

Parameters obtained by fitting the Argand χ_M"–χ_M' plots (H_{dc} = 3000 Oe, Figure S10) of **SmAu** using the generalized Debye model for single relaxation process. (Table S8) S18

Parameters obtained by fitting the temperature dependence of relaxation times (τ) presented as ln(τ) versus T^{-1} plots. (Table S9) S18

The outline of Nd^{III} compounds revealing single-molecule magnet behaviour. (Table S10) S19

Orientation of magnetic anisotropy (g_x, g_y, and g_z) for **NdAg**, **NdAu**, **SmAg**, and **SmAu**. (Figure S14) S20
CASSCF−SO results for the $^4F_{9/2}$ ground term of **NdAg**. (Table S11) S21
CASSCF−SO results for the $^4F_{9/2}$ ground term of **NdAu**. (Table S12) S21
CASSCF−SO results for the $^6H_{5/2}$ ground term of **SmAg**. (Table S13) S21
CASSCF−SO results for the $^6H_{5/2}$ ground term of **SmAu**. (Table S14) S21
Schematic for the removal of water from the equatorial position of Nd(III)/Sm(III) ion which was utilized as a input for the CASSCF-SO calculation (a-d), CASSCF–SO–computed energy levels of ground Kramer doublets for **NdAg** (e-h) and **SmAg** (i-l). (Figure S15) S22
CASSCF−SO results for the $^4F_{9/2}$ ground term of **NdAg** after removing one water molecule. (Table S15) S23
CASSCF−SO results for the $^4F_{9/2}$ ground term of **NdAg** after removing two water molecules. (Table S16) S23
CASSCF−SO results for the $^4F_{9/2}$ ground term of **NdAg** after removing three water molecules. (Table S17) S23
CASSCF−SO results for the $^6H_{5/2}$ ground term of **SmAg** after removing one water molecule. (Table S18) S23
CASSCF−SO results for the $^6H_{5/2}$ ground term of **SmAg** after removing two water molecules. (Table S19) S24
CASSCF−SO results for the $^6H_{5/2}$ ground term of **SmAg** after removing three water molecules. (Table S20) S24
The UV–VIS–NIR absorption spectra measured for **SmAu** and **SmAg** (a) as well as **NdAu** and **NdAg** (b) for the 250 – 1200 nm range. (Figure S16) S25
The solid-state temperature–dependent emission spectra of **NdAg** (a) and **SmAg** (c) along with excitation spectra of **NdAg** (b) and **SmAg** (d) in the shown temperature range. (Figure S17) S26
The temperature dependent excitation spectra of **NdAu** (a) and **SmAu** (b) recorded for emissive peak centred at 395 nm for **NdAu** and at 406 nm for **SmAu** in the indicated temperature range. (Figure S18) S27
The chromaticity colour diagram of **SmAg** and **SmAu** for excitation light of 325 nm. (Figure S19) S27
Summary of *xy* parameters of the CIE 1931 chromaticity scale for the emission colours of **SmAg** and **SmAu** detected at different temperature under indicated excitation wavelengths of excitation light. (Table S21) S28
List of the fitting parameters from Δ vs temperature plot for **SmAu** fitted with equation 2 given in the manuscript. (Table S22) S30
The summary of maximum and minimum calculated relative thermal sensitivity, S_r, and temperature uncertainty, ΔT, for **SmAu**. (Table S23) S30
Three cycles of repeatability data of thermometric parameters I_{430}/I_{400} and I_{430}/I_{590} of **SmAu** for 275 nm (a) and 365 nm (b) excitation light. (Figure S20) S31
References S31

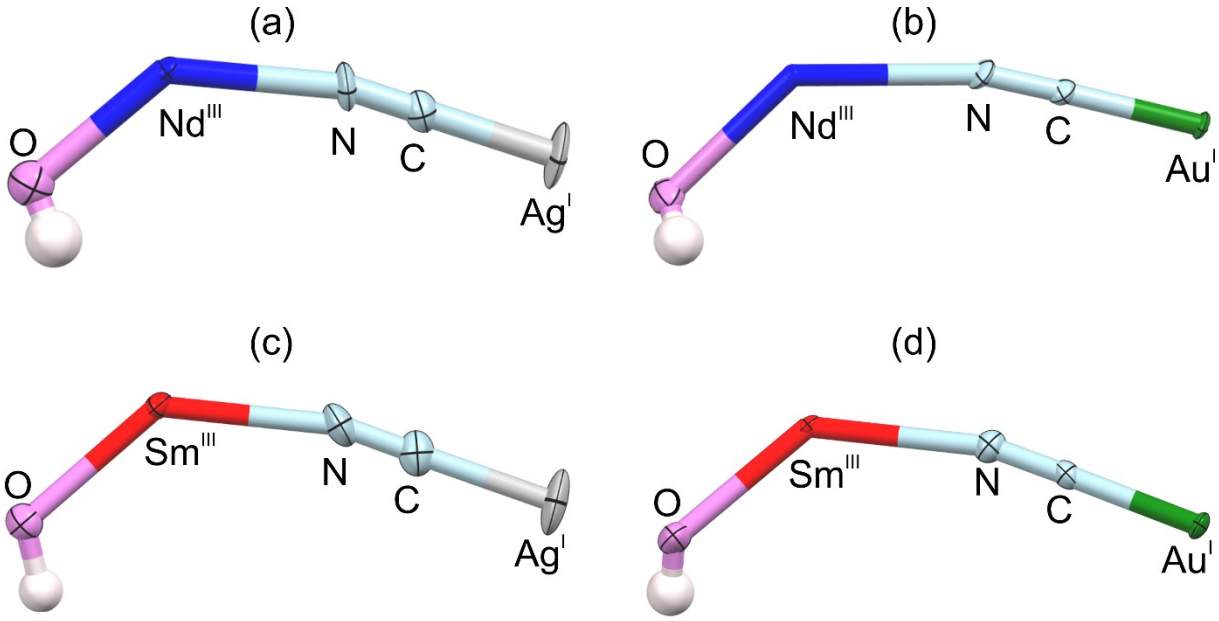

Figure S1. The representative asymmetric unit with atoms labelling of **NdAg**, **NdAu**, **SmAg**, and **SmAu**.

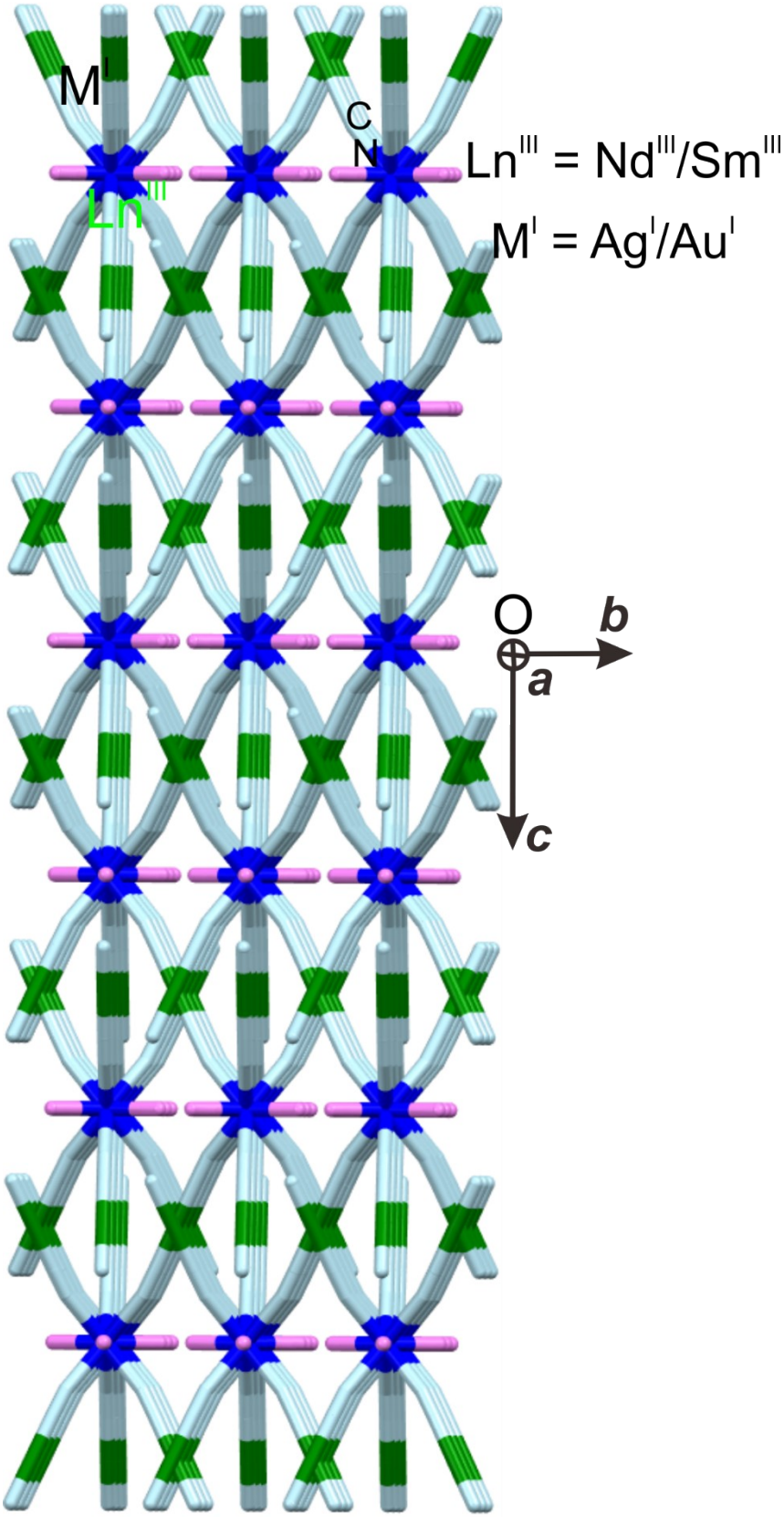

Figure S2. Representative view of the crystal packing of all four compounds along *ab*-plane.

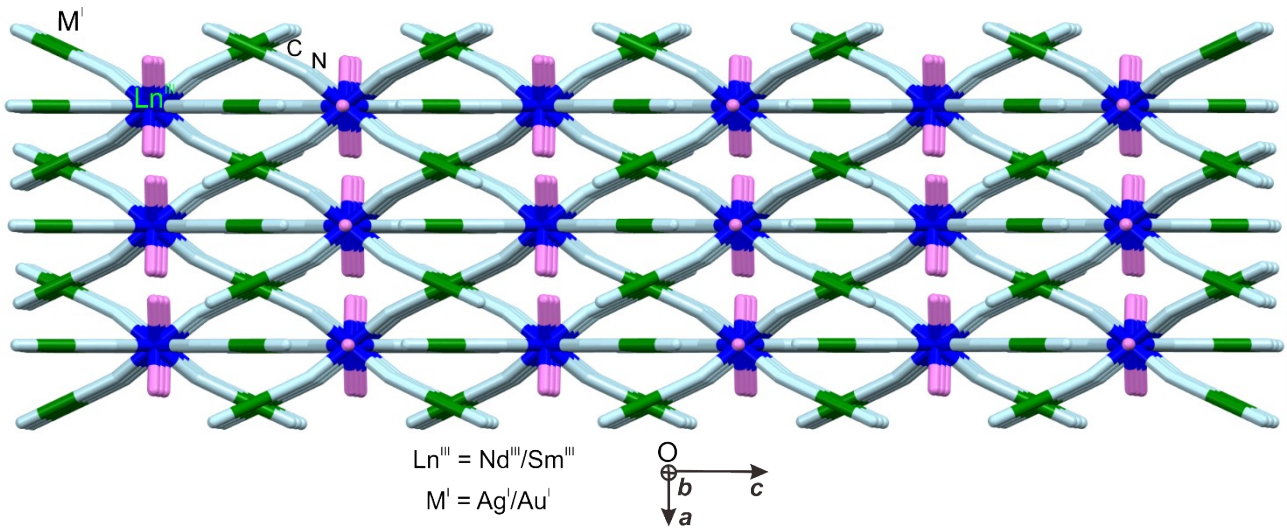

Figure S3. Representative view of the crystal packing of all four compounds along *ac*-plane.

Table S1. List of Selected bond lengths for **NdAg**, **NdAu**, **SmAg**, and **SmAu**.

Bond lengths [Å]				
	NdAg	**NdAu**	**SmAg**	**SmAu**
Nd1–N1	2.577(15)	2.595(5)		
Nd1–O1	2.49(3)	2.457(7)		
Ag1–C1	2.053(18)		2.058(9)	
Au1–C1		1.995(6)		1.996(5)
Sm1–N1			2.555(8)	2.567(4)
Sm1–O1			2.480(15)	2.434(6)
Nearest intermolecular Nd···Nd	6.712	6.568		
Nearest intermolecular Sm···Sm			6.648	6.551

Table S2. List of Selected bond angles for **NdAg** and **NdAu**.

Bond angles [°]		
	NdAg	**NdAu**
O1-Nd1-O1^{2}	120	120
O1^{1}-Nd1-O1	120	120
O1^{2}-Nd1-O1	120	120
O1-Nd1-N1^{3}	70.04(16)	70.04(4)
O1-Nd1-N1^{1}	70.04(15)	70.04(4)
O1^{1}-Nd1-N1	70.04(15)	70.04(4)
O1^{2}-Nd1-N1^{2}	133.0(4)	133.07(11)
O1^{1}-Nd1-N1^{3}	133.0(4)	133.07(11)
O1^{1}-Nd1-N1^{1}	133.0(4)	133.07(11)
O1^{2}-Nd1-N1^{1}	70.04(15)	70.04(4)
O1-Nd1-N1^{4}	133.0(4)	133.07(11)
O1-Nd1-N1^{2}	70.04(16)	70.04(4)
O1^{1}-Nd1-N1^{5}	70.04(15)	70.04(4)
O1^{1}-Nd1-N1^{2}	70.04(15)	70.04(4)
O1^{2}-Nd1-N1^{5}	133.0(4)	133.07(11)
O1^{1}-Nd1-N1^{4}	70.04(15)	70.04(4)
O1-Nd1-N1	133.0(4)	133.07(11)
O1^{2}-Nd1-N1	70.04(15)	70.04(4)
O1^{2}-Nd1-N1^{3}	70.04(15)	70.04(4)
O1^{2}-Nd1-N1^{4}	70.04(15)	70.04(4)
O1-Nd1-N1^{5}	70.04(15)	70.04(4)
N1^{5}-Nd1-N1^{1}	72.5(6)	72.51(17)
N1^{5}-Nd1-N1^{2}	93.9(8)	93.9(2)
N1^{4}-Nd1-N1^{5}	140.1(3)	140.07(8)
N1^{5}-Nd1-N1^{3}	140.1(3)	140.07(8)
N1^{1}-Nd1-N1^{2}	140.1(3)	140.07(8)
N1^{1}-Nd1-N1^{3}	93.9(8)	93.9(2)
N1^{4}-Nd1-N1	93.9(8)	93.9(2)
N1^{2}-Nd1-N1	140.1(3)	140.07(8)
N1^{1}-Nd1-N1	72.5(6)	72.51(17)
N1^{5}-Nd1-N1	72.5(6)	72.51(17)
N1^{4}-Nd1-N1^{1}	140.1(3)	140.07(8)
N1^{3}-Nd1-N1	140.1(3)	140.07(8)
N1^{3}-Nd1-N1^{2}	72.5(6)	72.51(17)
N1^{4}-Nd1-N1^{2}	72.5(6)	72.51(17)
N1^{4}-Nd1-N1^{3}	72.5(6)	72.51(17)
C1-N1-Nd1	166.7(16)	166.4(4)
N1-C1-Ag1	180(2)	
N1-C1-Au1		178.8(5)

^{1}-Y,+X-Y,+Z; ^{2}+Y-X,-X,3/2-Z; ^{3}+Y-X,-X,+Z; ^{4}-Y,+X-Y,3/2-Z; ^{5}+X,+Y,3/2-Z; ^{6}1-Y,+X-Y,+Z; ^{7}1-Y,1+X-Y,+Z; ^{8}1+Y-X,1-X,+Z; ^{9}+Y-X,1-X,+Z; ^{10}1-X,1-Y,1-Z

Table S3. List of Selected bond lengths and angles for **SmAg** and **SmAu**.

Bond angles [°]			
	SmAg		**SmAu**
O1-Sm1-O1^{1}	120.000(4)	**O1-Sm1-O1^{6}**	120
O1-Sm1-O1^{2}	120.000(4)	**O1-Sm1-O1^{7}**	120
O1-1Sm1-O1^{2}	120.000(5)	**O1^{6}-Sm1-O1^{7}**	120
O1-Sm1-N1	133.11(18)	**O1-Sm1-N1**	133.29(10)
O1-Sm1-N1^{3}	133.12(18)	**O1^{7}-Sm1-N1^{8}**	133.29(9)
O1^{1}-Sm1-N1	70.02(7)	**O1-Sm1-N1^{8}**	69.95(4)
O1-Sm1-N1^{1}	70.02(7)	**O1^{7}-Sm1-N1^{9}**	69.95(4)
O1^{2}-Sm1-N1	170.02(7)	**O1^{7}-Sm1-N1^{10}**	69.95(4)
O1^{2}-Sm1-N1	70.02(7)	**O1^{6}-Sm1-N1^{6}**	133.29(9)
O1^{1}-Sm1-N1	1133.12(18)	**O1^{6}-Sm1-N1^{8}**	69.95(4)
O1^{2}-Sm1-N1	370.02(7)	**O1^{6}-Sm1-N1**	69.95(4)
O1-1Sm1-N1	370.02(7)	**O1-Sm1-N1^{6}**	69.95(4)
N1-Sm1-N1^{3}	93.8(4)	**O1^{7}-Sm1-N1^{7}**	133.29(9)
N1-Sm1-N1^{1}	72.6(3)	**O1^{7}-Sm1-N1^{6}**	69.95(4)
N1^{3}-Sm1-N1^{1}	140.03(14)	**O1^{7}-Sm1-N1**	69.95(4)
O1B^{4}-Sm1-N1	132.27(18)	**O1^{6}-Sm1-N1^{9}**	69.95(4)
O1B^{1}-Sm1-N1	76.63(5)	**O1-Sm1-N1^{9}**	133.29(10)
O1B^{1}-Sm1-N1	76.63(5)	**O1-Sm1-N1^{7}**	69.95(4)
O1B^{4}-Sm1-N1	132.27(18)	**O1-Sm1-N11^{10}**	69.95(4)
O1B^{5}-Sm1-N1	76.63(5)	**O1^{6}-Sm1-N1^{7}**	69.95(4)
O1B^{2}-Sm1-N1	76.63(5)	**O1^{6}-Sm1-N11^{10}**	133.29(9)
O1B-Sm1-N1	132.27(18)	**N1^{1}-Sm1-N1^{8}**	72.86(15)
O1B^{6}-Sm1-N1	63.81(10)	**N1-Sm1-N1^{9}**	93.41(19)
O1B^{6}-Sm1-N1	132.27(18)	**N1-Sm1-N1^{8}**	139.90(7)
O1B^{4}-Sm1-N1	76.63(5)	**N1^{8}-Sm1-N1^{7}**	93.41(19)
O1B^{5}-Sm1-N1	63.81(9)	**N1^{7}-Sm1-N1^{6}**	72.86(15)
O1B^{2}-Sm1-N1	63.81(10)	**N1^{7}-Sm1-N1^{9}**	139.90(7)
O1B^{6}-Sm1-N1	63.81(10)	**N11^{10}-Sm1-N1^{6}**	93.41(19)
O1B^{1}-Sm1-N1	132.27(17)	**N1-Sm1-N11^{10}**	139.90(7)
O1B^{5}-Sm1-N1	76.63(5)	**N1^{8}-Sm1-N1^{9}**	72.86(15)
O1B-Sm1-N1^{3}	132.27(18)	**N11^{10}-Sm1-N1^{9}**	72.86(15)
O1B^{2}-Sm1-N1	63.81(10)	**N1^{6}-Sm1-N1^{9}**	139.90(7)
O1B-Sm1-N1^{1}	63.81(10)	**N1-Sm1-N1^{6}**	72.86(15)
O1B^{5}-Sm1-O1B^{1}	140.5	**N11^{10}-Sm1-N1^{7}**	139.90(8)
O1B-Sm1-O1B^{2}	120	**N1-Sm1-N1^{7}**	72.86(15)
O1B^{6}-Sm1-O1B^{2}	99.5	**N1^{8}-Sm1-N1^{6}**	139.90(8)
O1B^{2}-Sm1-O1B^{1}	120	**C1-N1-Sm1**	165.9(4)
O1B^{4}-Sm1-O1B^{2}	140.5	**N1-C1-Au1**	179.3(5)
O1B-Sm1-O1B^{4}	20.5		
O1B^{2}-Sm1-O1B^{5}	20.5		
O1B-Sm1-O1B^{1}	120		
O1B^{4}-Sm1-O1B^{1}	99.5		
O1B-Sm1-O1B^{6}	140.5		
O1B^{6}-Sm1-O1B^{1}	20.5		

O1B-Sm1-O1B[5]	99.5		
O1B6-Sm1-O1B5	120		
O1B4-Sm1-O1B6	120		
O1B4-Sm1-O1B5	120		
C1-N1-Sm1	165.9(8)		
N1-C1-Ag1	179.2(10)		
N1-C1-Au1			

SmAg: [1]-Y,+X-Y,+Z; [2]+Y-X,-X,3/2-Z; [3]+Y-X,-X,+Z; [4]-Y,+X-Y,3/2-Z; [5]+X,+Y,3/2-Z; [6]1-Y,+X-Y,+Z; [7]1-Y,1+X-Y,+Z; [8]1+Y-X,1-X,+Z; [9]+Y-X,1-X,+Z; [10]1-X,1-Y,1-Z

SmAu: [1]1-Y,+X-Y,+Z; [2]1-Y,1+X-Y,+Z; [3]1+Y-X,1-X,+Z; [4]+Y-X,1-X,+Z; [5]1-X,1-Y,1-Z; [6]1+Y-X,2-X,+Z; [7]2-Y,1+X-Y,+Z; [8]2-Y,1+X-Y,3/2-Z; [9]+X,+Y,3/2-Z; [10]1+Y-X,2-X,3/2-Z

Table S4. Results of Continuous Shape Measure (CSM) analysis for **NdAg**, **NdAu**, **SmAg**, and **SmAu** compounds for $[Ln^{III}(H_2O)(CN)_6]^{3-}$-moiety.

compound	**CSM parameters***					**geometry**
	JCSAPR-9	CSAPR-9	JTCTPR-9	MFF-9	TCTPR-9	
NdAg	2.432	1.066	2.775	1.895	0.056	**CSAPR-9**
NdAu	2.588	1.100	3.045	1.916	0.097	**CSAPR-9**
SmAg	2.393	1.053	2.698	1.883	0.055	**CSAPR-9**
SmAu	2.562	1.080	2.978	1.892	0.106	**CSAPR-9**

*CSM parameters:[1, 2]

CSM JCSAPR-9 = the parameter related to the Capped square antiprism (C_{4v} symmetry)

CSM CSAPR-9 = the parameter related to the Spherical capped square antiprism (C_{4v} symmetry)

CSM JTCTPR-9 = the parameter related to the Tricapped trigonal prism (D_{3h} symmetry)

CSM TCTPR-9 = the parameter related to the Spherical tricapped trigonal prism (D_{3h} symmetry)

CSM MFF-9 = the parameter related to the Muffin (Cs symmetry)

CSM = 0 for the ideal geometry and increases with the increasing distortion from the ideal polyhedron.

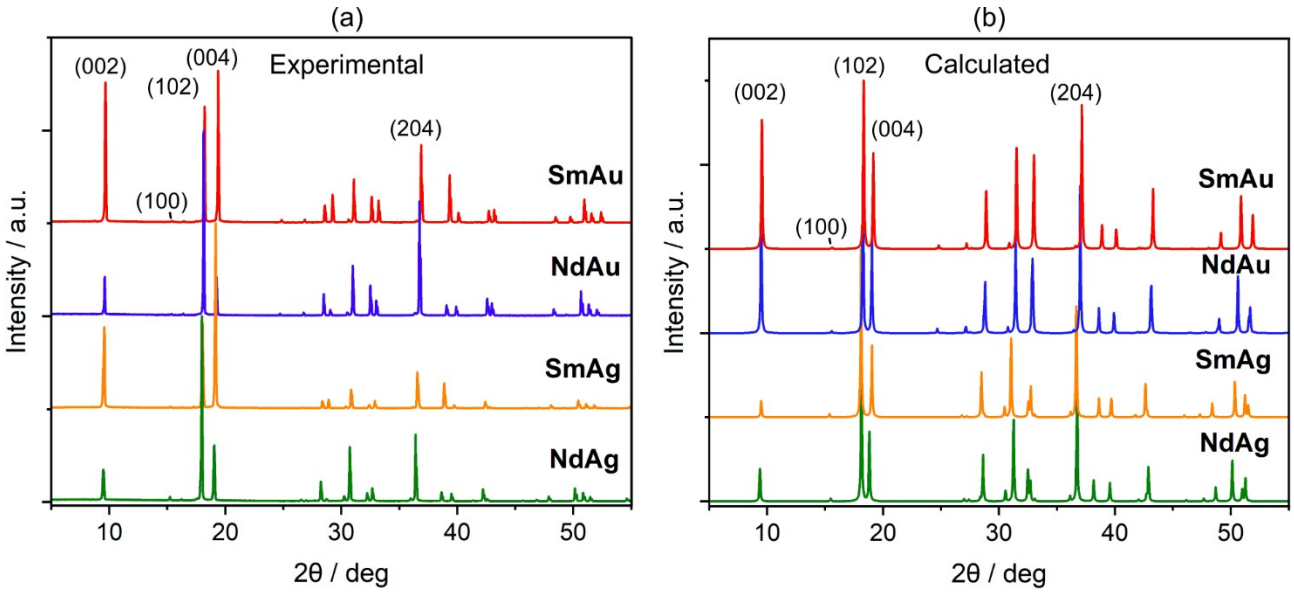

Figure S4. Experimental powder X-ray diffraction patterns of **NdAg**, **NdAu**, **SmAg**, and **SmAu** (a) compared with the calculated X-ray diffraction patterns obtained from the corresponding single crystal X-ray diffraction analyses of **NdAg**, **NdAu**, **SmAg**, and **SmAu** (b) in the broad 5–55° range of 2*Θ*. The number above the peaks shows the miller indices responsible for the respective maxima.

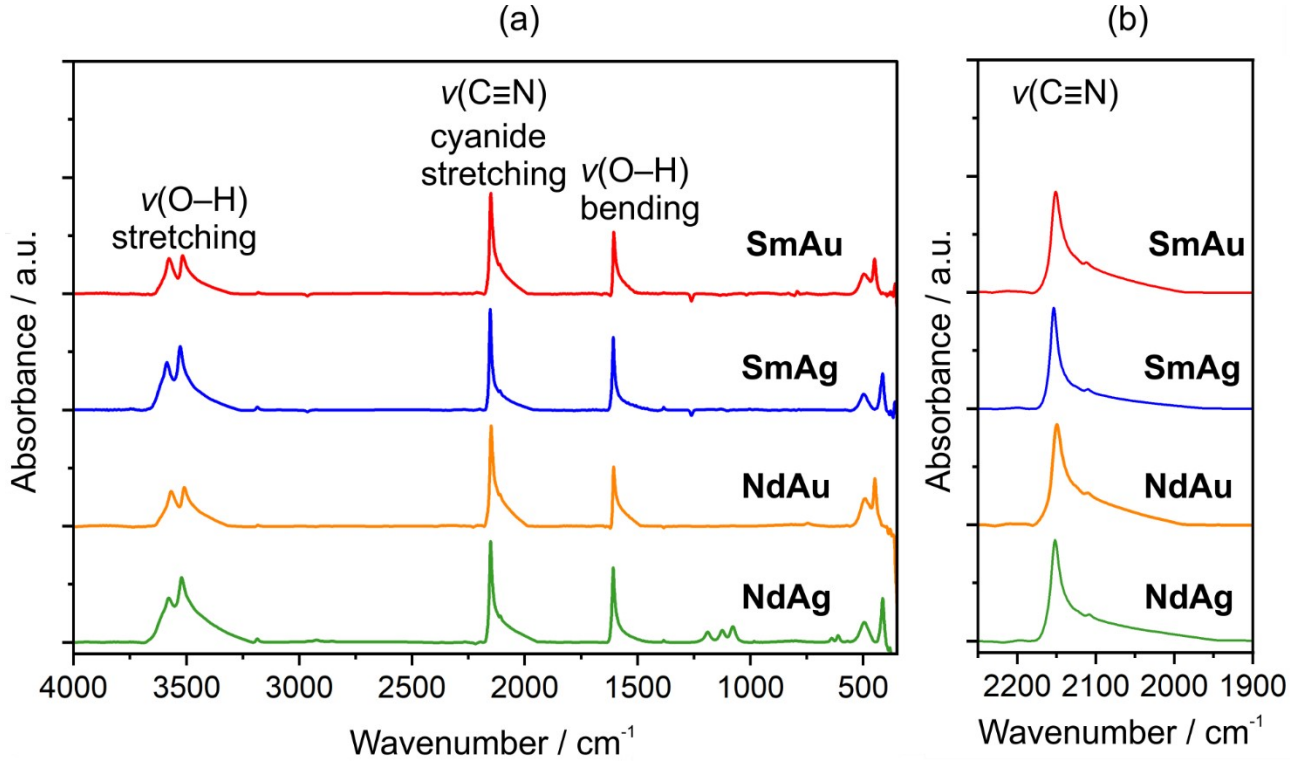

Figure S5. The infrared spectroscopy (IR) for **NdAg**, **NdAu**, **SmAg**, and **SmAu** measured in the KBr matrix for the measurement range of 4000 – 350 cm^{-1} (a) and 2250 – 1900 cm^{-1} (b).

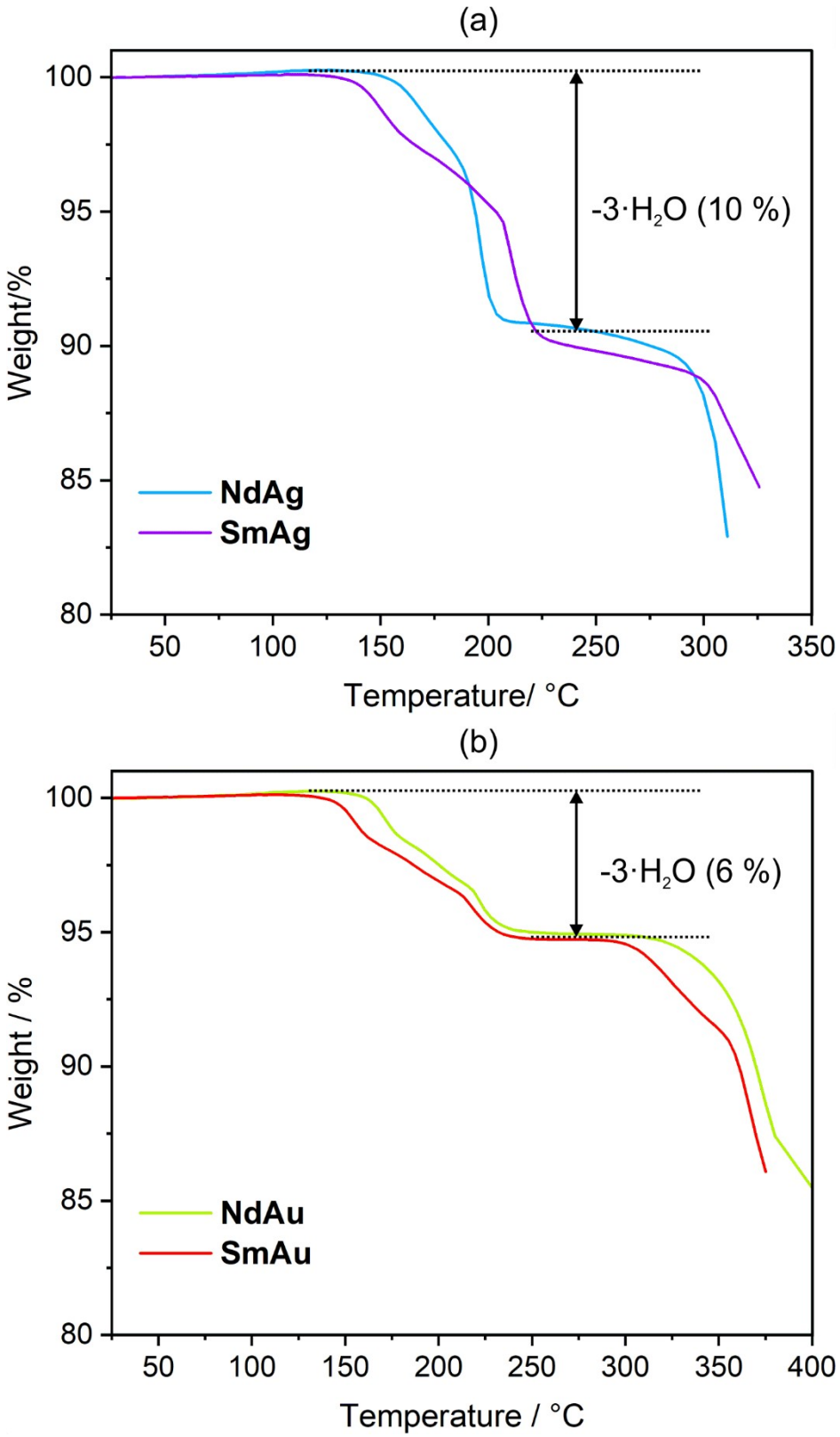

Figure S6. Thermogravimetric curves of molecular frameworks with Ag(I) ion **NdAg** and **SmAg** (upper part) along with the Au(I) containing compounds **NdAu** and **SmAu** measured in air atmosphere for indicated temperature range with the shown steps concerning mass loss ascribed to the removal of water molecules.

Comment Related to Figure S6:

The 3–D polymeric framework of **NdAg**, **NdAu**, **SmAg**, and **SmAu** have high thermal stability up to almost 145, 145, 125, and 125°C, respectively (Figure S6). The larger thermal stability is observed for the Sm(III) containing assemblies than for the Nd(III) having compounds by 25°C. Further heating the sample starts the removal of three water molecules in three subsequent steps with an overall mass loss of around 10 % for Ag(I) containing compounds and 6 % for the Au(I) having materials. All water molecules are removed under standard atmospheric conditions by around 220 K for all the assemblies.

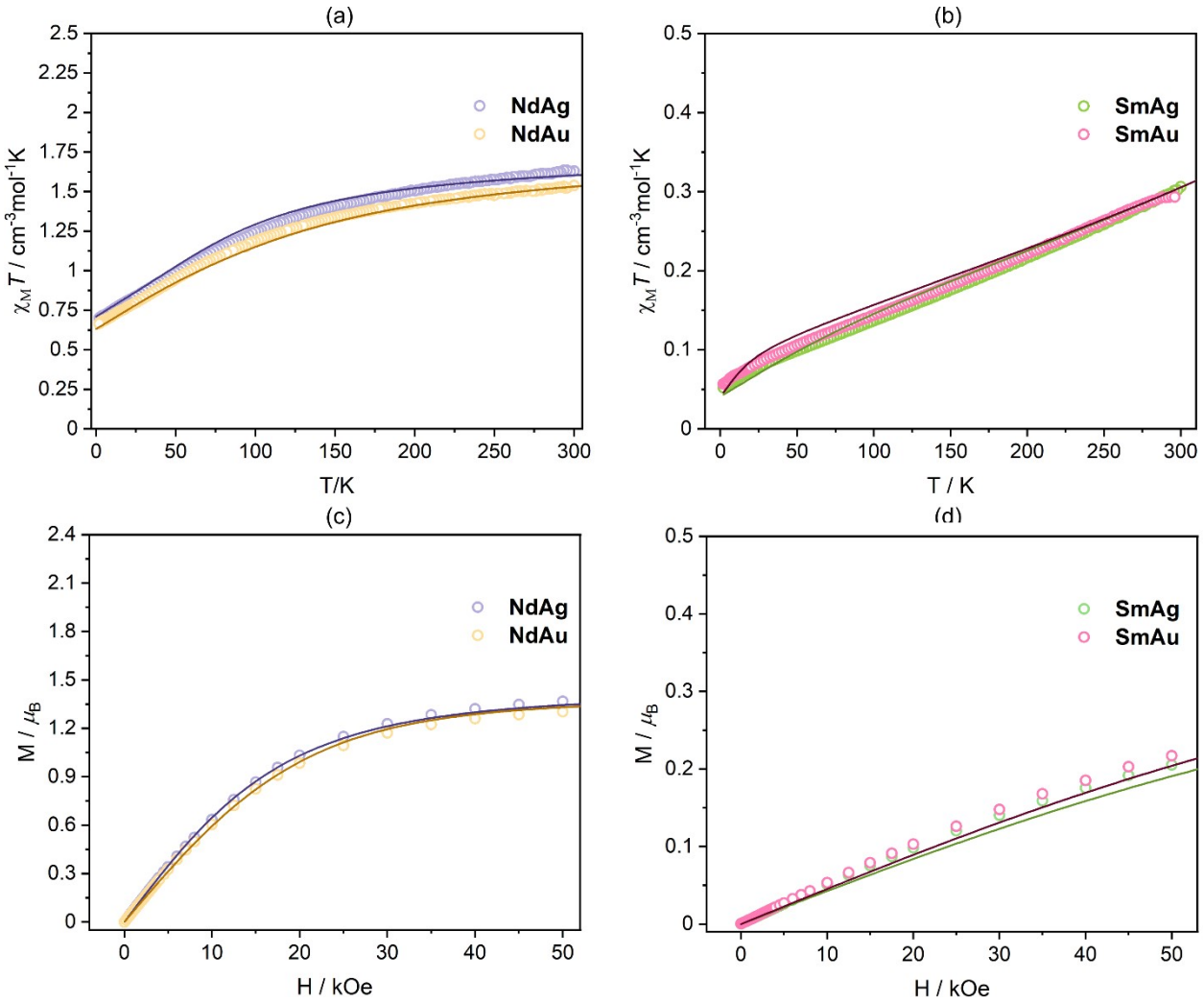

Figure S7. Temperature-dependent product of temperature with molar magnetic susceptibility (χ_MT) for Nd(III)-having compound (a) and Sm(III)-containing compounds (b) along with field dependence magnetization (*M-H*) data (c and d). The experimental data is denoted by the open circles and solid lines are calculated fitted line with the computed magnetization values using CASSCF/RASSI-SO results.

The following equations of the generalized Debye model for the single relaxation process were applied:

$$\chi'(\omega) = \chi_S + (\chi_T - \chi_S)\frac{1 + (\omega\tau)^{1-\alpha}\sin\left(\pi\alpha/2\right)}{1 + 2(\omega\tau)^{1-\alpha}\sin\left(\pi\alpha/2\right) + (\omega\tau)^{2(1-\alpha)}} \qquad \textbf{E1}$$

$$\chi''(\omega) = (\chi_T - \chi_S)\frac{(\omega\tau)^{1-\alpha}\cos\left(\pi\alpha/2\right)}{1 + 2(\omega\tau)^{1-\alpha}\sin\left(\pi\alpha/2\right) + (\omega\tau)^{2(1-\alpha)}} \qquad \textbf{E2}$$

where

χ_S = the adiabatic susceptibility (at an infinitely high frequency of *ac* field),

χ_T = the isothermal susceptibility (at an infinitely low frequency of *ac* field),

τ = the relaxation time,

α = the distribution (Cole-Cole) parameter,

and ω is an angular frequency, that is $\omega = 2\pi\nu$, with ν standing for the linear frequency in [Hz] units.[3]

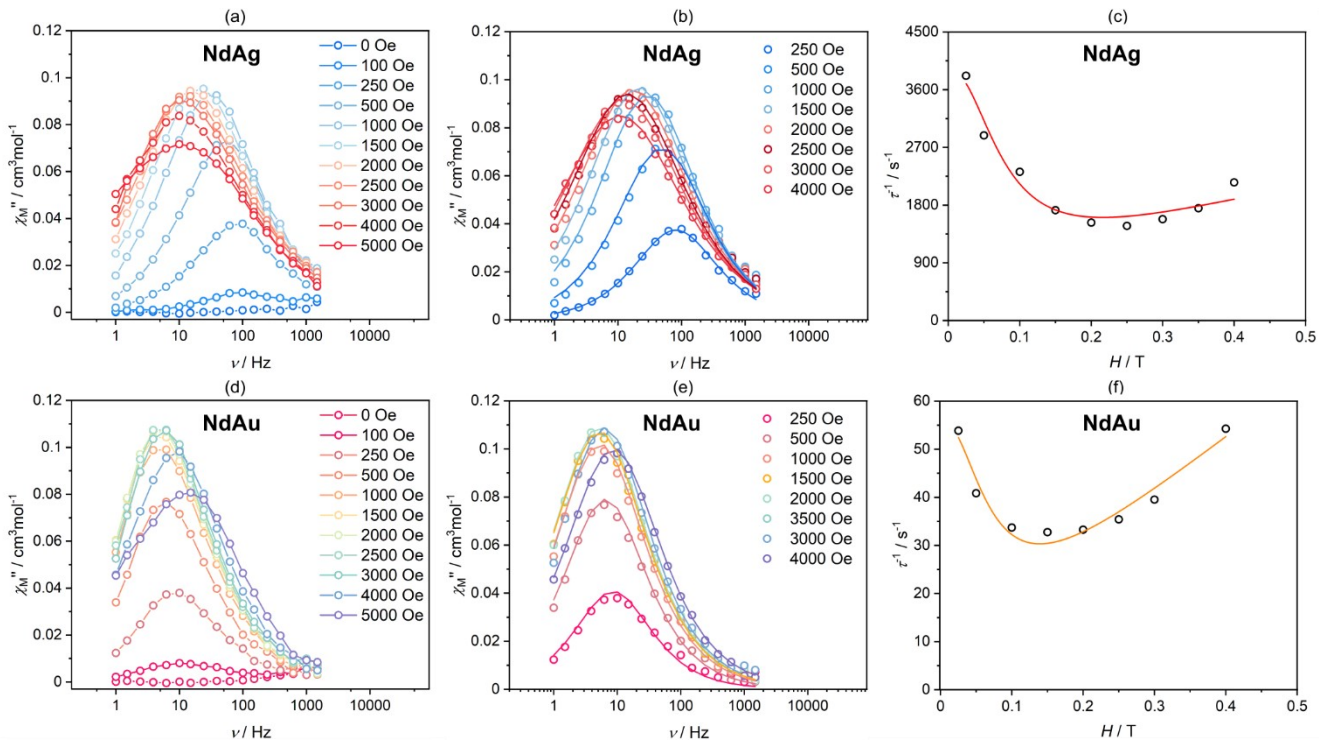

Figure S8. Overlapped frequency dependencies of out–of–plane χ_M'' magnetic susceptibility for **NdAg** (a;b) and **NdAu** (d;e) in H_{ac} = 3 Oe at T = 1.85 K for given external *dc* magnetic fields. The experimental dotted plots (Figure S8b, d) are fitted with the general-Debye model for a single relaxation process to extract the relaxation time corresponding to each applied *dc* magnetic field, which is plotted in Figure S8c and f, respectively, for **NdAg** and **NdAu**. Solid lines in Figure S8a and d are only to guide the eye. The

fitting of plots in Figure S8c and f, is done by equation 2 given in Table S9 considering field-dependent quantum tunnelling of magnetization and direct relaxation processes.

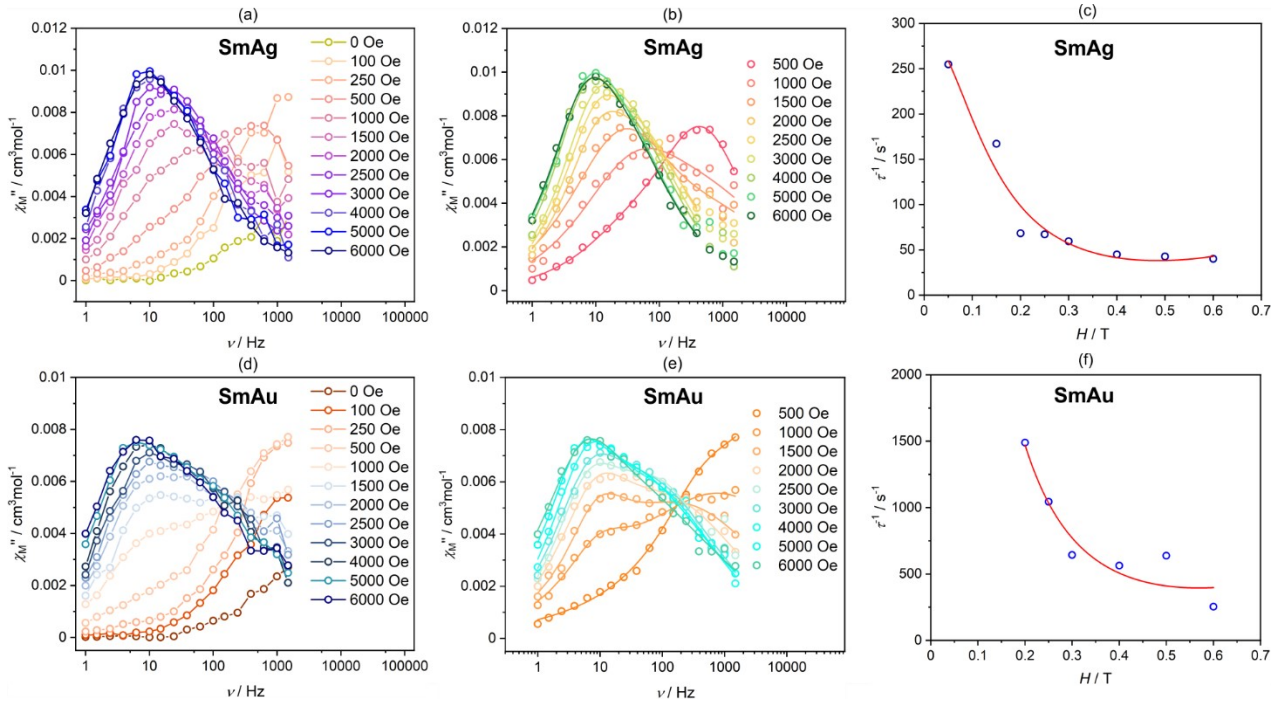

Figure S9. Overlapped frequency dependencies of out–of–plane χ_M" magnetic susceptibility for **SmAg** (a;b) and **SmAu** (c;d) in H_{ac} = 3 Oe at T = 1.85 K for given external *dc* magnetic fields. The experimental dotted plots (Figure S9b, d) are fitted with the general-Debye model for a single relaxation process to extract the relaxation time corresponding to each applied *dc* magnetic field, which is plotted in Figure S9c and f, respectively, for **SmAg** and **SmAu**. The solid lines in Figure S9a and c are only to guide the eye. The fitting of plots in Figure S9c and f, is done by equation 2 given in Table S9, considering field-dependent quantum tunnelling of magnetization and direct relaxation processes.

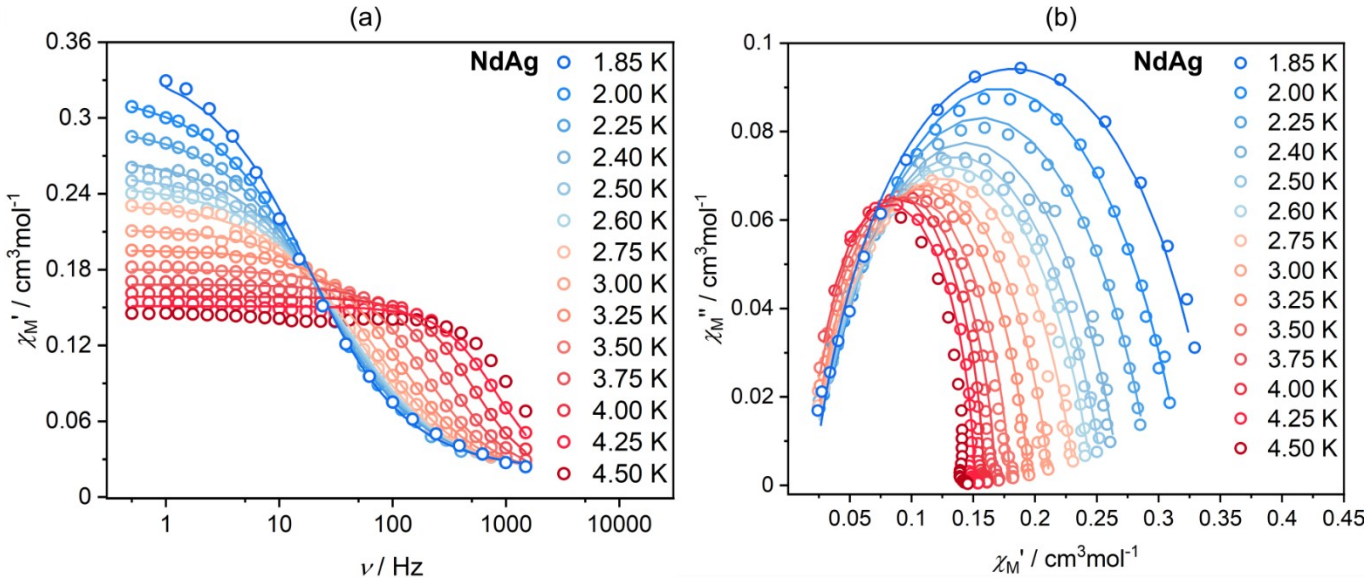

Figure S10. *Ac* magnetic properties of the **NdAg**, for H_{dc} = 2000 Oe and H_{ac} = 3 Oe: variation of in-plane, χ_M' (a) frequency components of the compound magnetic susceptibility and the related χ_M''–χ_M' Argand plots (b) for the given temperatures of the 1.85–4.50 K range. The open circle represents the experimental data, and solid lines are fitted curves using the general-Debye model for a single relaxation process.

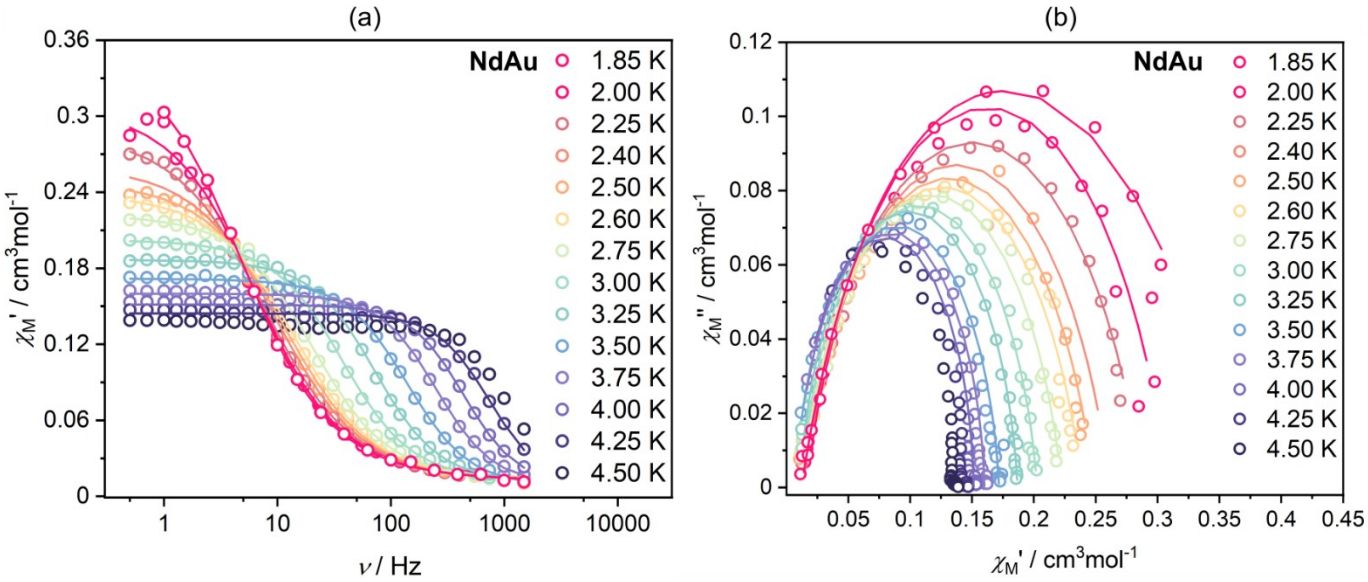

Figure S11. *Ac* magnetic properties of the **NdAu**, for H_{dc} = 2000 Oe and H_{ac} = 3 Oe: variation of in-plane, χ_M' (a) frequency components of the compound magnetic susceptibility and the related χ_M''–χ_M' Argand plots (b) for the given temperatures of the 1.85–4.50 K range. The open circle represents the experimental data and solid lines are fitted curves using the general-Debye model for a single relaxation process.

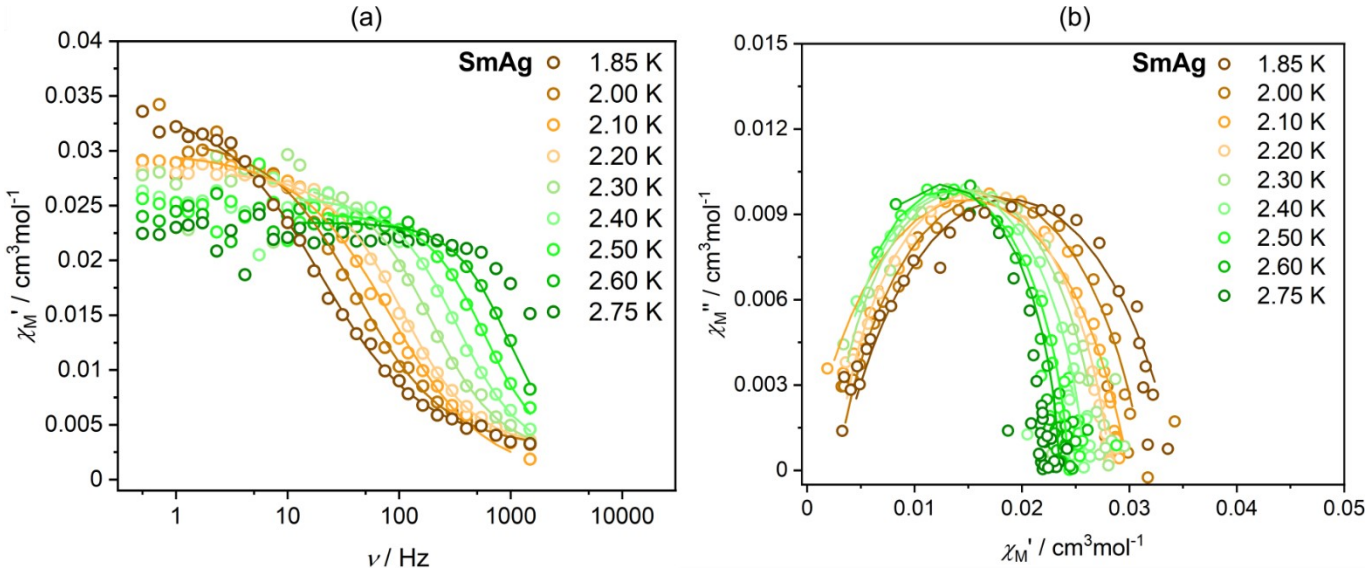

Figure S12. *Ac* magnetic properties of the **SmAg**, for H_{dc} = 3000 Oe and H_{ac} = 3 Oe: variation of in-plane, χ_M' (a) frequency components of the compound magnetic susceptibility and the related χ_M''–χ_M' Argand plots (b) for the given temperatures of the 1.85–2.75 K range. The open circle represents the experimental data and solid lines are fitted curves using the general-Debye model for a single relaxation process.

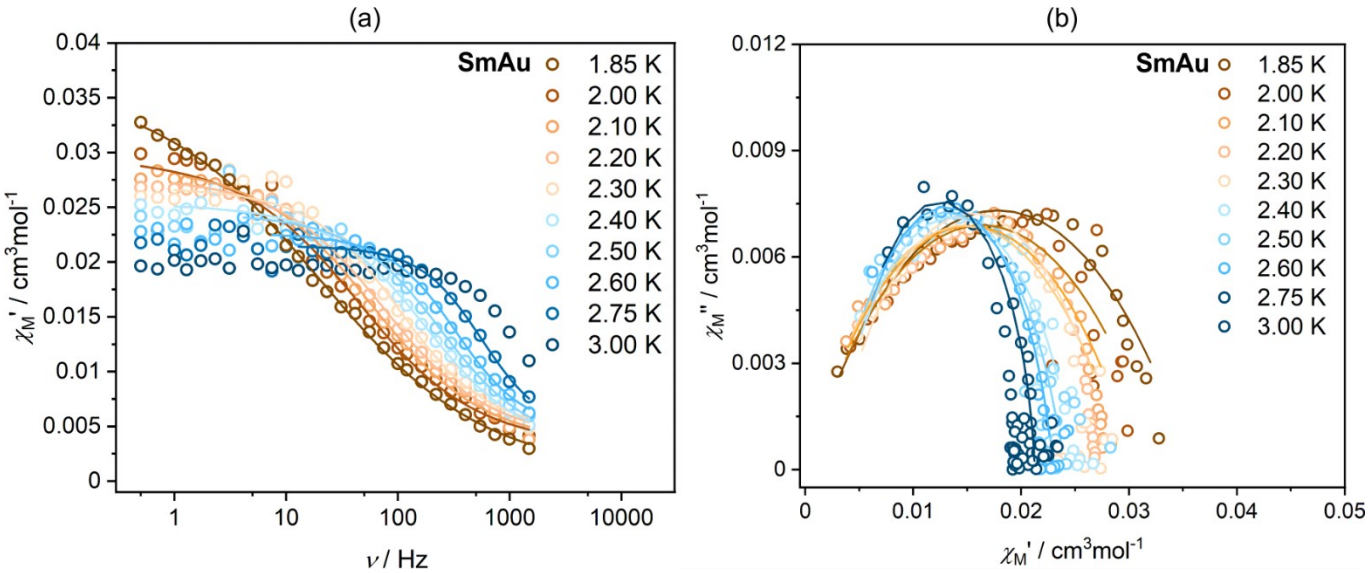

Figure S13. *Ac* magnetic properties of the **SmAu**, for H_{dc} = 3000 Oe and H_{ac} = 3 Oe: variation of in-plane, χ_M' (a) frequency components of the compound magnetic susceptibility and the related χ_M''–χ_M' Argand plots (b) for the given temperatures of the 1.85–3.00 K range. The open circle represents the experimental data and solid lines are fitted curves using the general-Debye model for a single relaxation process.

Table S5. Parameters obtained by fitting the Argand χ_M"–χ_M' plots (H_{dc} = 2000 Oe, Figure S10) of **NdAg** using the generalized Debye model for a single relaxation process.

***T* / K**	χ_S **cm^{3}mol^{-1}**	χ_T **cm^{3}mol^{-1}**	***τ* / s**	***α***
1.85	0.0050655	0.136965	0.008852	0.172863
2.00	0.0202474	0.320768	0.007951	0.313822
2.25	0.0179222	0.294964	0.006536	0.311552
2.40	0.0195749	0.26921	0.005172	0.292553
2.50	0.0187202	0.255979	0.004465	0.286545
2.60	0.0169873	0.247016	0.003924	0.288072
2.75	0.0166087	0.232955	0.003199	0.272706
3.00	0.0170803	0.212201	0.002157	0.227069
3.25	0.017636	0.195431	0.001391	0.177673
3.50	0.0154916	0.180198	0.00084	0.144344
3.75	0.0158112	0.168116	0.000512	0.097929
4.00	0.0157198	0.158769	0.000313	0.05916
4.25	0.0127078	0.151022	0.000192	0.050566

Table S6. Parameters obtained by fitting the Argand χ_M"–χ_M' plots (H_{dc} = 2000 Oe, Figure S11) of **NdAu** using the generalized Debye model for a single relaxation process.

***T* / K**	χ_S **cm^{3}mol^{-1}**	χ_T **cm^{3}mol^{-1}**	***τ* / s**	***α***
1.85	0.0050655	0.136965	0.008852	0.172863
2.00	0.0158032	0.308664	0.024989	0.223374
2.25	0.0129927	0.287889	0.021155	0.242498
2.40	0.013177	0.261426	0.015784	0.221813
2.50	0.012838	0.248809	0.013267	0.216503
2.60	0.012213	0.239043	0.011259	0.210041
2.75	0.0126147	0.222414	0.007817	0.178299
3.00	0.0115699	0.202581	0.004275	0.142984
3.25	0.0109263	0.186808	0.00221	0.104342
3.50	0.007021	0.171817	0.001152	0.098696
3.75	0.0089909	0.160009	0.000635	0.059894
4.00	0.0083565	0.151298	0.000363	0.036446
4.25	0.0064438	0.144322	0.000215	0.032673

Table S7. Parameters obtained by fitting the Argand χ_M''–χ_M' plots (H_{dc} = 3000 Oe, Figure S12) of **SmAg** using the generalized Debye model for a single relaxation process.

T / K	χ_S cm^{3}mol^{-1}	χ_T cm^{3}mol^{-1}	τ / s	α
1.85	0.002955	0.0344194	0.008092	0.306017
2.00	0.002754	0.0313919	0.003854	0.2446
2.10	5.29732E-12	0.0299224	0.001903	0.278249
2.25	0.00271729	0.0282213	0.001522	0.167731
2.30	0.00210124	0.0273333	0.000843	0.152054
2.40	0.00190497	0.0258711	0.000473	0.120596
2.50	0.00193409	0.0243114	0.000271	0.07931
2.60	0.00161168	0.0234683	0.000163	0.053005

Table S8. Parameters obtained by fitting the Argand χ_M''–χ_M' plots (H_{dc} = 3000 Oe, Figure S13) of **SmAu** using the generalized Debye model for a single relaxation process.

T / K	χ_S cm^{3}mol^{-1}	χ_T cm^{3}mol^{-1}	τ / s	α
1.85	1.08309E-08	0.0353723	0.007312	0.507848
2.00	0.00275433	0.0313919	0.003854	0.2446
2.10	5.29732E-12	0.0299224	0.001903	0.278249
2.25	0.00271729	0.0282213	0.001522	0.167731
2.30	0.00241809	0.0285139	0.001446	0.355819
2.40	0.00232256	0.0250679	0.000811	0.287132
2.50	0.00214329	0.023977	0.000557	0.252518
2.60	0.00313707	0.0229623	0.000426	0.181808
2.75	0.00384668	0.0212623	0.000267	0.089451

Table S9. Parameters obtained by fitting the temperature dependence of relaxation times (τ) presented as ln(τ) versus T^{-1} plots using the indicated equations provided in the manuscript.

Equation 1	$\tau^{-1} = A_{direct}H^mT + \frac{B_1}{(1+B_2H^2)} + B_{raman}T^n$						
Parameters	A_{direct}(s^{-1} Oe^{m-} K^{-1})	m	B_1(s^{-1})	B_2(Oe^{2-})	B_{raman}(s^{-n}K^{-1})	n	R^2
NdAg	120.6	0.64	455.8	164.5	0.0032	10.0	0.9903
NdAu	64.55	0.94	91.2	200.0	0.0026	9.9	0.9975
SmAg	351.3	2.76	290.0	40.0	0.0149	13.5	0.9993
SmAu	380.0	2.49	1182.9	92.7	0.0902	10.4	0.9965
Equation 2	$\tau^{-1} = A_{direct}H^mT + \frac{B_1}{(1+B_2H^2)}$						
NdAg	1724.4	0.65	3757.7	164.5			0.9560
NdAu	64.45	0.93	54.7	200.7			0.9472
SmAg	60.9	2.76	290.7	49.8			0.9551
SmAu	380.0	2.49	6752.1	90.7			0.9011

Table S10. The outline of Nd^{III} compounds revealing single-molecule magnet behaviour. The energy barrier and relaxation times for **NdAg** and **NdAu** are obtained by fitting experimental data with Arrhenius law ($\ln(\tau) = \Delta E/k_B T + \ln(\tau_0)$) from the high-temperature range relaxation times.

compound	$\Delta E/k_B$ / K	τ_0 / s	H_{dc} / Oe	Ref.
three-dimensional molecular coordination networks/polymers				
$[Nd^{III}(H_2O)_3][Ag^{I}(CN)_2]_3$ (NdAg)	18.8	3.80×10^{-6}	2000	This work
$[Nd^{III}(H_2O)_3][Au^{I}(CN)_2]_3$ (NdAu)	25.5	7.22×10^{-7}	2000	This work
zero-dimensional molecular systems				
$[Nd^{III}(TTA)_3(MeOH)_2]\cdot 0.5$Azo-py	19.7(7)	$3.7(8)\cdot 10^{-7}$	2000	4
$[Li(dme)_3][Nd^{III}(COT'')_2]$ (dme = dimethoxyethane; COT'' = bis(trimethylsilyl)cyooctatetraenyl dianion)	21	$5.5\cdot 10^{-5}$	1000	5
$[Nd^{III}(Tp)_3]$ (Tp = trispyrazolylaborate)	4.1(1)	$4.2(2)\cdot 10^{-5}$	100	6
$[Nd^{III}(^{t}BuPO(NH^{i}Pr)_2)_2(H_2O)_5]I_3\cdot H_2O$	24.69 16.08 39.21	$5.03\cdot 10^{-6}$ $2.64\cdot 10^{-6}$ $8.98\cdot 10^{-6}$	0 0 2000	7
$Na_9[Nd^{III}(W_5O_{18})_2]$	73.9	$3.55\cdot 10^{-10}$	1000	8
$[Nd^{III}(NO_3)_3$(18-crown-6)]	33.4(5)	$1.6(2)\cdot 10^{-9}$	1000	9
$[Nd^{III}(NO_3)_3$(1,10-diaza-18-crown-6)]	73(2)	$1.4(6)\cdot 10^{-10}$	1000	9
$(NH_2Me_2)_3\{[Nd^{III}(Mo_4O_{13})(dmf)_4]_3(btc)_2\}\cdot 8(dmf)$ (btc = 1,3,5-benzentricarboxylate anion)	34.06	$4.69\cdot 10^{-8}$	500	10
$[Nd^{III}(Cp^*)_2](BPh_4)$ (Cp* = pentamethylcyclopentadienyl anion)	41(2)	$1.4(4)\cdot 10^{-6}$	1000	11
$[Nd(ntfa)_3(phen)]$ (ntfa = 4,4,4-trifluoro-1-(naphthalen-2-yl)butane-1,3-dionate, phen = phenanthroline)	25.9	2.2×10^{-7}	1500	12
$[Nd(ntfa)_3(bipy)]$ (ntfa = 4,4,4-trifluoro-1-(naphthalen-2-yl)butane-1,3-dionate, bipy = 2,2′-dipyridine)	44.6	1.0×10^{-9}	1500	12
one-dimensional coordination polymers				
$[Nd^{III}_2(CNCH_2COO)_6(H_2O)_4]\cdot 2H_2O$	26.6(1)	$1.75\cdot 10^{-7}$	1500	13
$\{[Nd^{III}(pzdo)(H_2O)_4][Co^{III}(CN)_6]\}\cdot 0.5(pzdo)\cdot 4H_2O$	51(2)	$4.5(9)\cdot 10^{-8}$	1000	14
$[Nd^{III}(3,5\text{-dnb})_3(H_2O)_2]\cdot MeCN$ (3,5-dnb = 3,5-dinitrobenzoic acid anion)	27	$4.1\cdot 10^{-7}$	2000	15
$[Nd^{III}(2,4\text{-dnb})_2(CH_3COO)(H_2O)_2]$ (2,4-dnb = 2,4-dinitrobenzoic acid anion)	29	$3.1\cdot 10^{-7}$	3500	15
$\{Nd(\alpha\text{-fur})_3(H_2O)_2\}$ (α-fur = C_4H_3OCOO)	121(2)	$1.04\cdot 10^{-13}$	1200	16
$\{Nd_{0.065}La_{0.935}(\alpha\text{-fur})_3(H_2O)_2\}_n$ (α-fur = C_4H_3OCOO)	61(2)	$3.63\cdot 10^{-11}$	1200	16

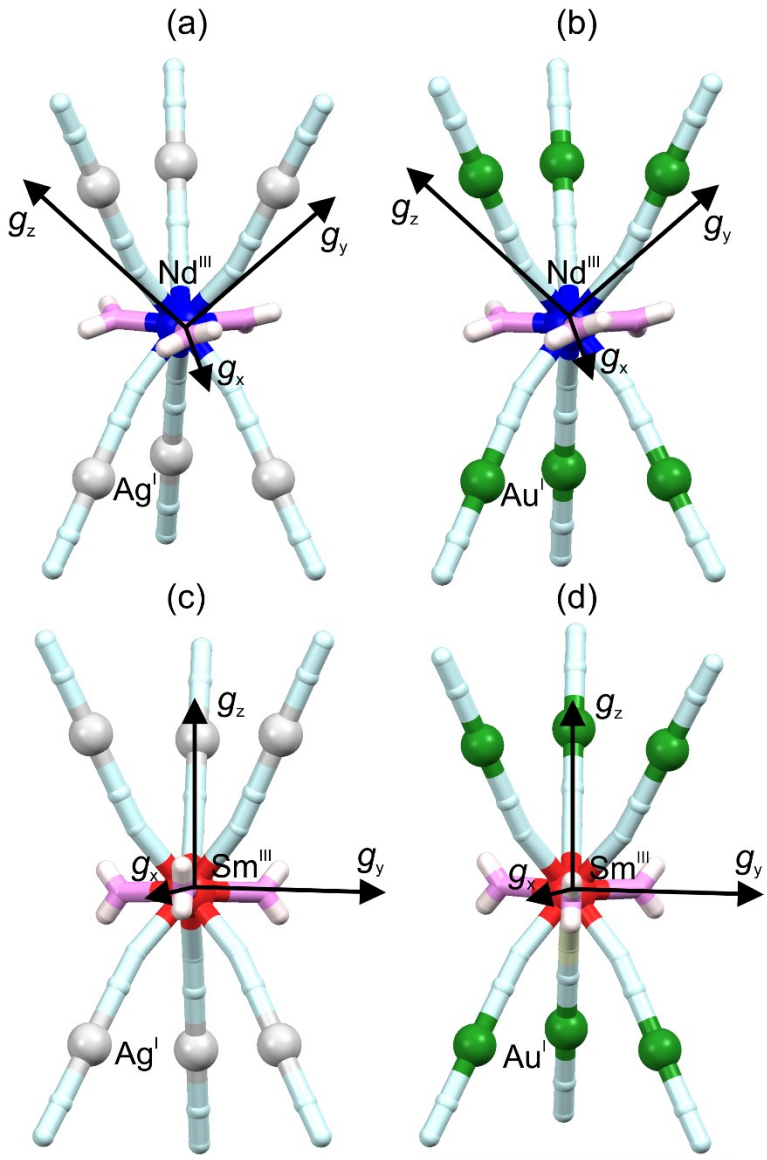

Figure S14. Orientation of magnetic anisotropy (g_x, g_y, and g_z) for **NdAg**, **NdAu**, **SmAg**, and **SmAu**. The above structure is also used as an input file to evaluate the lanthanide-centric properties.

Table S11. CASSCF−SO results for the $^4F_{9/2}$ ground term of **NdAg**.

Energy [cm^{-1}]	g_x	g_y	g_z	CF wave function composition	$\langle J_z \rangle$
0.0	2.51	2.57	2.70	36.6 % |±9/2⟩ + 10.7 % |±5/2⟩ + 42.0 % |±1/2⟩	**±1.353**
123.0	0.13	0.46	2.78	18.3 % |±9/2⟩ + 38.8 % |∓7/2⟩ + 9.7 % |±5/2⟩ + 35.7 % |±3/2⟩	**±0.443**
200.1	3.55	3.14	0.42	30.6 % |±7/2⟩ + 31.4 % |∓5/2⟩ + 31.5 % |±3/2⟩ + 17.0 % |±1/2⟩	**±1.178**
355.8	2.90	2.88	1.11	27.3 % |±9/2⟩ + 14.2 % |∓5/2⟩ + 36.5 % |±3/2⟩ + 19.7 % |±1/2⟩	**±0.855**
379.9	0.05	0.09	2.03	19.1 % |±9/2⟩ + 20.0 % |∓7/2⟩ + 34.0 % |±5/2⟩ + 20.8 % |±1/2⟩ + 6.1 % |±3/2⟩	**±0.279**

Table S12. CASSCF−SO results for the $^4F_{9/2}$ ground term of **NdAu**.

Energy [cm^{-1}]	g_x	g_y	g_z	CF wave function composition	$\langle J_z \rangle$
0.0	2.51	2.57	2.70	34.3 % |±9/2⟩ + 13.8 % |±5/2⟩ + 35.1 % |±1/2⟩	**±1.348**
122.3	0.14	0.49	2.72	19.5 % |±9/2⟩ + 41.5 % |∓7/2⟩ + 14.1 % |±5/2⟩ + 21.3 % |±3/2⟩	**±0.268**
196.9	3.56	3.11	0.40	19.6 % |±7/2⟩+ 34.0 % |∓5/2⟩ + 30.7 % |±3/2⟩ + 15.3 % |±1/2⟩	**±1.308**
355.1	2.90	2.89	1.09	25.8 % |±9/2⟩+ 10.9 % |∓5/2⟩ + 29.4 % |±3/2⟩ + 27.9 % |±1/2⟩	**±0.945**
379.1	0.048	0.09	2.10	17.5 % |±9/2⟩+ 27.9 % |∓7/2⟩ + 27.0 % |±5/2⟩ + 18.3 % |±1/2⟩ + 9.2 % |±3/2⟩	**±0.185**

Table S13. CASSCF−SO results for the $^6H_{5/2}$ ground term of **SmAg**.

Energy [cm^{-1}]	g_x	g_y	g_z	CF wave function composition	$\langle J_z \rangle$
0.0	0.71	0.71	0.56	100 % |±1/2⟩	**±0.28**
35.8	1.08 x 10^{-5}	0.007	0.89	100 % |±3/2⟩	**±0.45**
77.7	0.22	0.22	1.52	100 % |±5/2⟩	**±0.76**

Table S14. CASSCF−SO results for the $^6H_{5/2}$ ground term of **SmAu**.

Energy [cm^{-1}]	g_x	g_y	g_z	CF wave function composition	$\langle J_z \rangle$
0.0	0.71	0.71	0.55	100 % |±1/2⟩	**±0.28**
35.8	1.24 x 10^{-5}	0.007	0.88	100 % |±3/2⟩	**±0.44**
77.7	0.21	0.21	1.51	100 % |±5/2⟩	**±0.76**

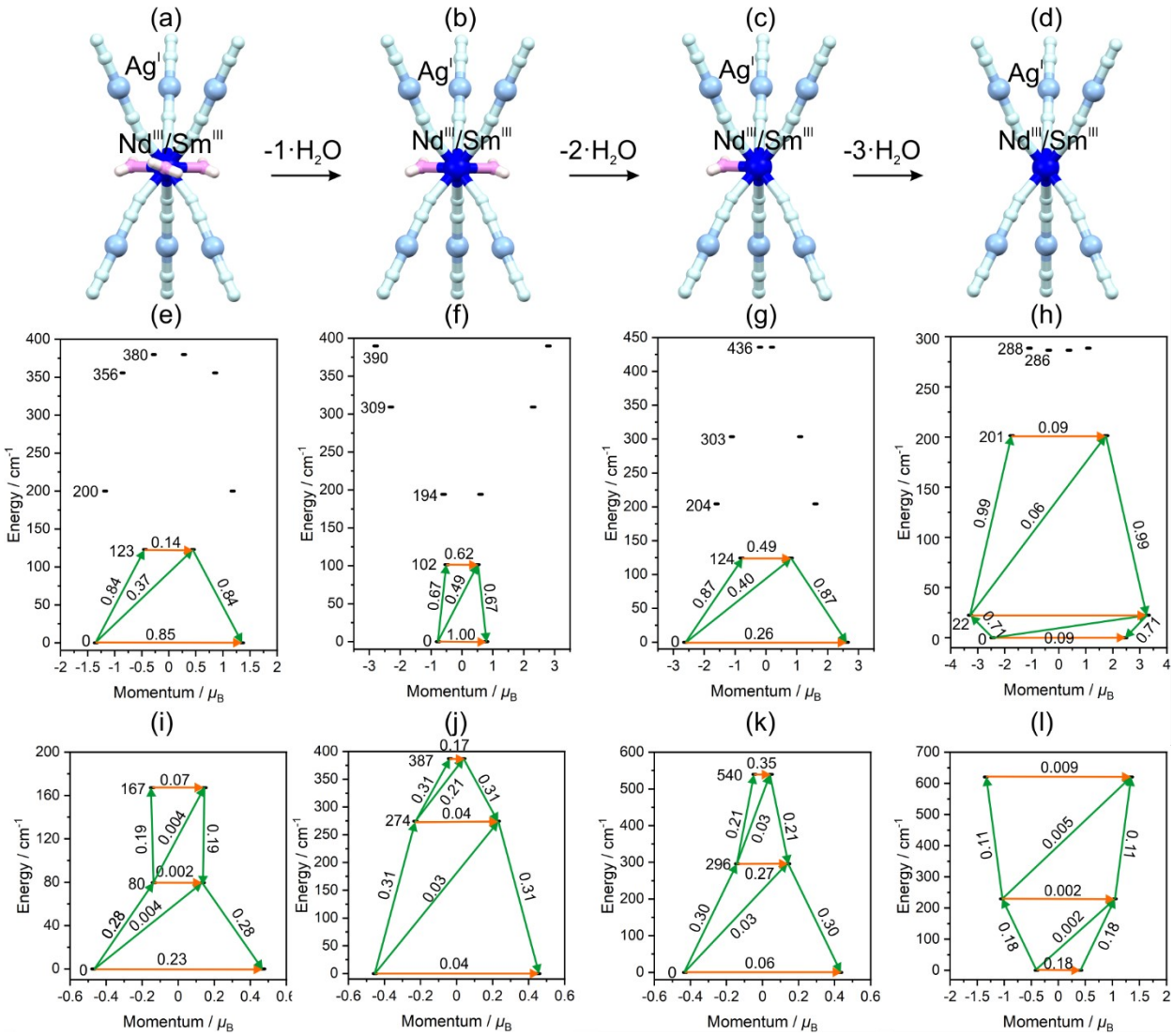

Figure S15. Schematic for the removal of water from the equatorial position of Nd(III)/Sm(III) ion which was utilized as an input for the CASSCF-SO calculation (a-d), CASSCF–SO–computed energy levels of ground Kramer doublets for **NdAg** (e-h) and **SmAg** (i-l) corresponding to structure with subsequent removal of water molecules. They show magnetic–dipole transition probability in the absence of an external magnetic field calculated from the average of three cartesian transition magnetic moment operators. The number on the top of connecting lines is the normalized transition probability.

Table S15. CASSCF−SO results for the $^4F_{9/2}$ ground term of **NdAg** after removing one water molecule.

Energy [cm^{-1}]	g_x	g_y	g_z	CF wave function composition	$\langle J_z \rangle$
0.0	3.28	2.75	1.56	54.8 % |±5/2⟩ + 38.0 % |±3/2⟩	**±0.779**
101.6	2.79	2.60	0.40	10.0 % |±7/2⟩ + 37.3 % |∓5/2⟩ + 49.6 % |±3/2⟩	**±0.495**
194.3	1.18	1.87	4.48	12.7 % |±9/2⟩ + 81.3 % |∓1/2⟩	**±0.598**
309.2	0.34	1.80	4.62	84.8 % |±7/2⟩	**±2.303**
389.8	0.07	0.30	5.59	82.0 % |±9/2⟩ + 11.6 % |∓1/2⟩	**±2.792**

Table S16. CASSCF−SO results for the $^4F_{9/2}$ ground term of **NdAg** after removing two water molecules.

Energy [cm^{-1}]	g_x	g_y	g_z	CF wave function composition	$\langle J_z \rangle$
0	0.33	1.22	5.23	67.2 % |±9/2⟩ + 24.9 % |±5/2⟩	**±2.616**
124.4	0.79	1.05	3.19	17.5 % |±7/2⟩ + 52.1 % |∓3/2⟩ + 21.9 % |±1/2⟩	**±0.795**
204.3	1.26	2.10	3.90	18.0 % |±9/2⟩ + 20.9 % |∓3/2⟩ + 34.1 % |±5/2⟩ + 20.6 % |±5/2⟩	**±1.602**
303.4	1.54	2.17	3.72	52.6 % |±7/2⟩ + 25.0 % |∓5/2⟩ + 11.9 % |±3/2⟩	**±1.108**
435.9	0.28	0.35	6.44	15.0 % |±5/2⟩ + 28.2 % |∓3/2⟩ + 47.9 % |∓1/2⟩	**±0.192**

Table S17. CASSCF−SO results for the $^4F_{9/2}$ ground term of **NdAg** after removing three water molecules.

Energy [cm^{-1}]	g_x	g_y	g_z	CF wave function composition	$\langle J_z \rangle$
0	0.26	0.26	4.91	99.8 % |±7/2⟩	**±2.453**
22.4	8.6 x 10^{-7}	1.4 x 10^{-6}	6.57	100.0 % |±9/2⟩	**±3.283**
201.5	0.28	0.28	3.49	99.9 % |±5/2⟩	**±1.746**
286.5	3.62	3.62	0.75	100.0 % |±1/2⟩	**±0.375**
288.6	4.9 x 10^{-5}	9.5 x 10^{-5}	2.18	99.9 % |±3/2⟩	**±1.088**

Table S18. CASSCF−SO results for the $^6H_{5/2}$ ground term of **SmAg** after removing one water molecule.

Energy [cm^{-1}]	g_x	g_y	g_z	CF wave function composition	$\langle J_z \rangle$
0.0	0.062	0.184	0.907	97.8 % |±5/2⟩	**±0.453**
274.4	0.595	0.575	0.456	82.3 % |±3/2⟩ + 15.9 % |∓1/2⟩	**±0.228**
387.0	0.029	0.424	1.549	16.2 % |±3/2⟩ + 83.4 % |∓1/2⟩	**±0.037**

Table S19. CASSCF−SO results for the $^6H_{5/2}$ ground term of **SmAg** after removing two water molecules.

Energy [cm^{-1}]	g_x	g_y	g_z	**CF wave function composition**	$\langle J_z \rangle$
0.0	0.043	0.313	0.861	92.2 % $\lvert\pm5/2\rangle$ + 7.1 % $\lvert\mp1/2\rangle$	**±0.430**
295.8	0.284	0.470	1.139	87.9 % $\lvert\pm3/2\rangle$ + 9.3 % $\lvert\mp1/2\rangle$	**±0.142**
539.6	0.075	0.091	2.023	11.4 % $\lvert\pm3/2\rangle$ + 83.7 % $\lvert\mp1/2\rangle$	**±0.046**

Table S20. CASSCF−SO results for the $^6H_{5/2}$ ground term of **SmAg** after removing three water molecules.

Energy [cm^{-1}]	g_x	g_y	g_z	**CF wave function composition**	$\langle J_z \rangle$
0.0	0.54	0.54	0.81	100 % $\lvert\pm1/2\rangle$	**±0.405**
295.8	4.0 x 10^{-7}	0.007	2.09	100 % $\lvert\pm3/2\rangle$	**±1.043**
539.6	0.03	0.03	2.68	100 % $\lvert\pm5/2\rangle$	**±1.341**

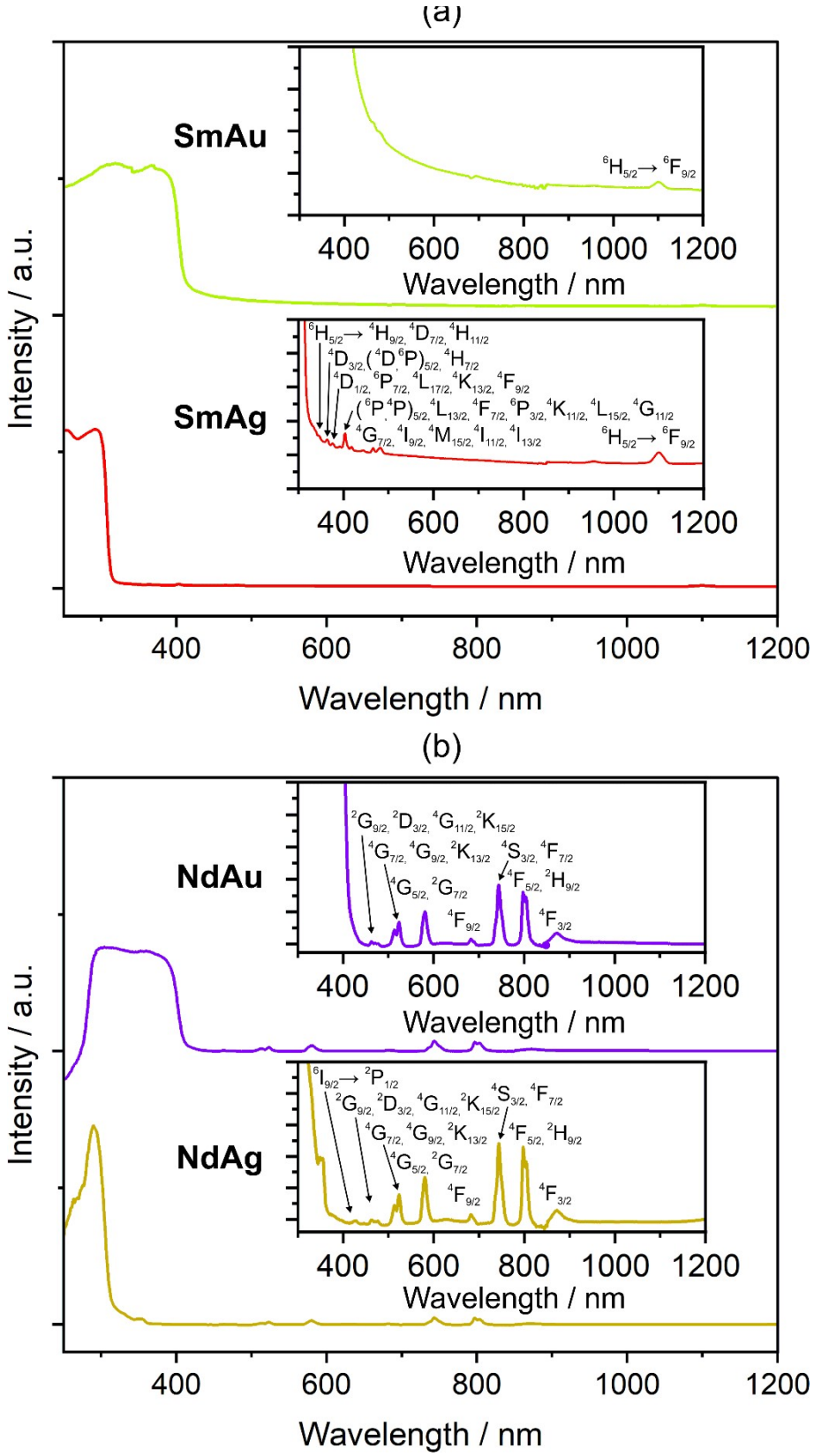

Figure S16. The UV–VIS–NIR absorption spectra measured for **SmAu** and **SmAg** (a) as well as **NdAu** and **NdAg** (b) for the 250 – 1200 nm range. The inset of each spectrum contains the enlarged view of spectra from 300 – 1200 nm.

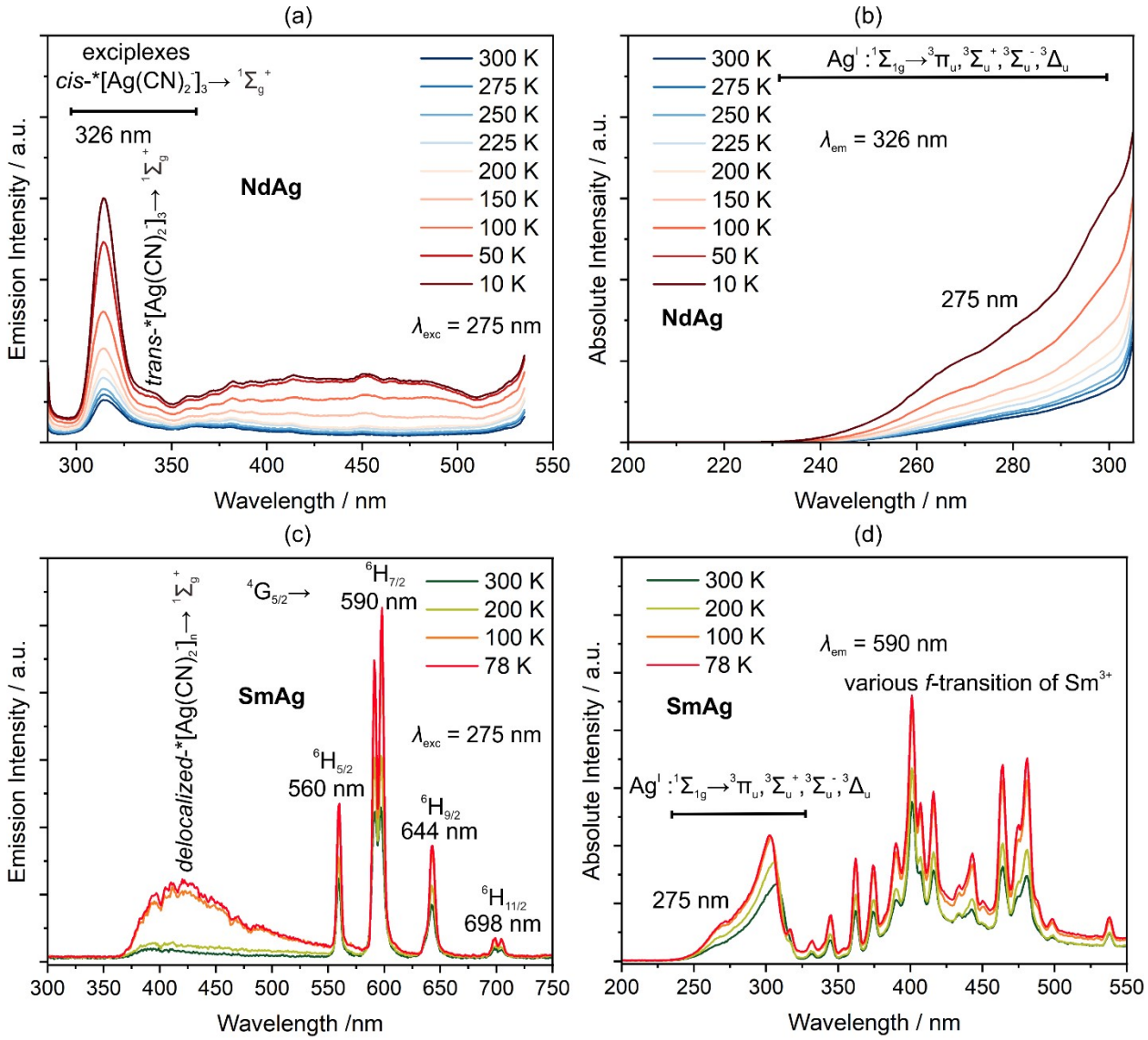

Figure S17. The solid-state temperature-dependent emission spectra of **NdAg** (a) and **SmAg** (c) along with excitation spectra of **NdAg** (b) and **SmAg** (d) in the shown temperature range. The emission spectra are measured for 275 nm excitation light and excitation spectra are recorded for 326 nm emission peak of **NdAg** and 590 emission peak of **SmAg**.

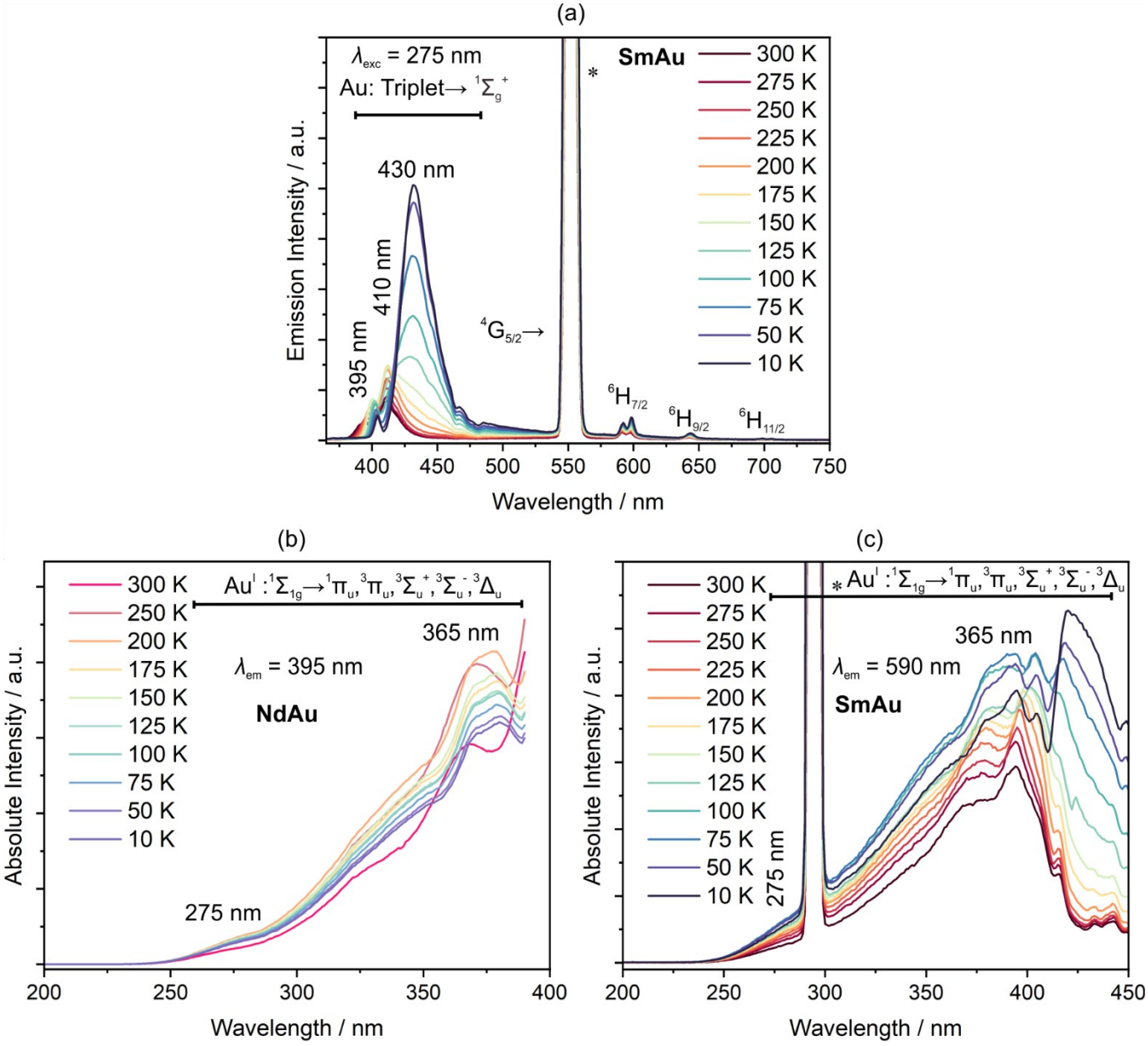

Figure S18. The temperature-dependent emission spectra of **SmAu** (a), and excitation spectra of **NdAu** (b) and **SmAu** (c) recorded for indicated excitation (for part a) and emissive peaks (for part b and c) in the indicated temperature range. Star-marked peaks suggest the presence of a second-order Rayleigh scattered peak at 295 nm.

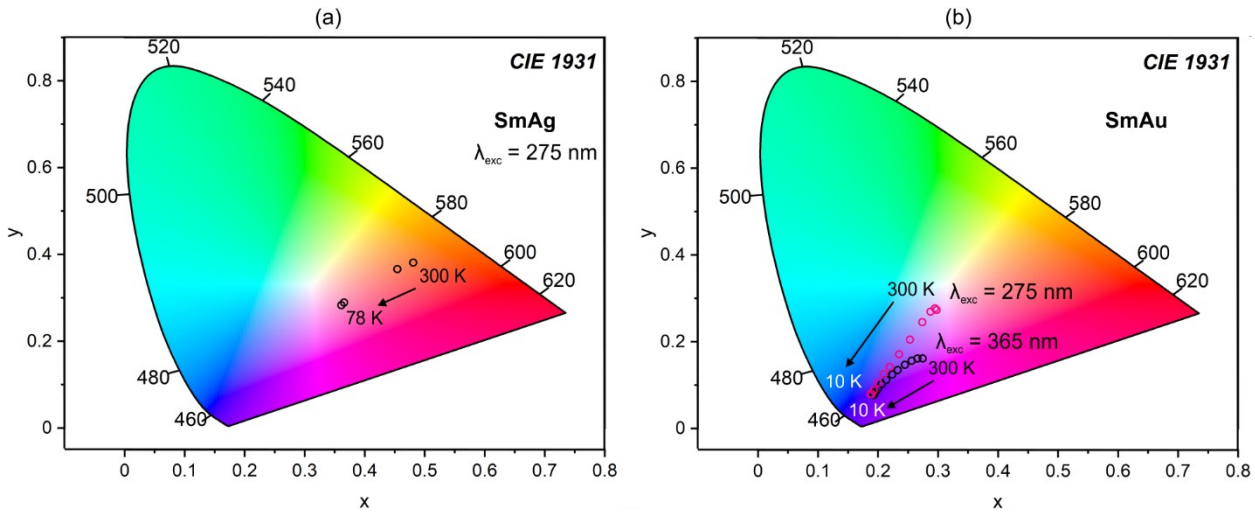

Figure S19. The chromaticity colour diagram of **SmAg** and **SmAu** for excitation light of 325 nm.

Table S21. Summary of *xy* parameters of the CIE 1931 chromaticity scale for the emission colours of **SmAg** and **SmAu** detected at a different temperature under indicated excitation wavelengths of excitation light.

Compound	Temperature	Wavelength	*x*	*y*
SmAg	300 K	275 nm	0.48074	0.3811
	200 K	275 nm	0.45423	0.36611
	100 K	275 nm	0.36555	0.28926
	78 K	275 nm	0.36099	0.28309
SmAu	300 K	275 nm	0.2976	0.27323
	275 K	275 nm	0.29464	0.27681
	250 K	275 nm	0.28732	0.26928
	225 K	275 nm	0.27379	0.24525
	200 K	275 nm	0.25308	0.20492
	175 K	275 nm	0.23491	0.17116
	150 K	275 nm	0.21957	0.14193
	125 K	275 nm	0.20916	0.12524
	100 K	275 nm	0.19974	0.10522
	75 K	275 nm	0.19277	0.08815
	50 K	275 nm	0.18887	0.07953
	10 K	275 nm	0.18788	0.07998
SmAu	300 K	365 nm	0.27432	0.16168
	275 K	365 nm	0.26551	0.1612
	250 K	365 nm	0.25592	0.15617
	225 K	365 nm	0.24477	0.14678
	200 K	365 nm	0.23268	0.13474
	175 K	365 nm	0.22353	0.12436
	150 K	365 nm	0.21383	0.11188
	125 K	365 nm	0.20594	0.10242
	100 K	365 nm	0.19991	0.09252
	75 K	365 nm	0.19589	0.08448
	50 K	365 nm	0.19331	0.07872
	10 K	365 nm	0.19242	0.07693

Table S22. List of the fitting parameters from Δ vs temperature plot for **SmAu** fitted with equation 2 given in the manuscript.

Compounds	Excitation Wavelength	parameter	Δ(430/400)	Δ(430/590)
SmAu	**275 nm**	α_1	2.0	1.4
		$\Delta E_1/k_B$	73.2	91.3
		α_2	300.0	89.0
		$\Delta E_2/k_B$	404.5	485.1
		Δ_0	34.8	21.7
		$R^2(COD)$	0.999	0.996
SmAu	**365 nm**	α_1	2.0	3.1
		$\Delta E_1/k_B$	54.6	131.2
		α_2	93.5	54.5
		$\Delta E_2/k_B$	310.1	589.1
		Δ_0	15.3	15.1
		$R^2(COD)$	0.999	0.999

Table S23. The summary of maximum and minimum calculated relative thermal sensitivity, S_r, and temperature uncertainty, ΔT, for **SmAu**.

Compound	Excitation Wavelength	parameters	Δ(430/400)	Δ(430/590)
SmAu	**275 nm**	S_r (max., % K^{-1})	3.50@80 K	1.78@110 K
		S_r (min., % K^{-1})	0.10@10 K	0.01@10 K
		ΔT (max., K)	0.37@300 K	0.47@300 K
		ΔT (min., K)	0.01@100 K	0.05@100 K
SmAu	**365 nm**	S_r (max., % K^{-1})	2.67@70 K	1.08@130 K
		S_r (min., % K^{-1})	0.32@300 K	0.001@10 K
		ΔT (max., K)	0.49@300 K	0.55@300 K
		ΔT (min., K)	0.02@100 K	0.13@75 K

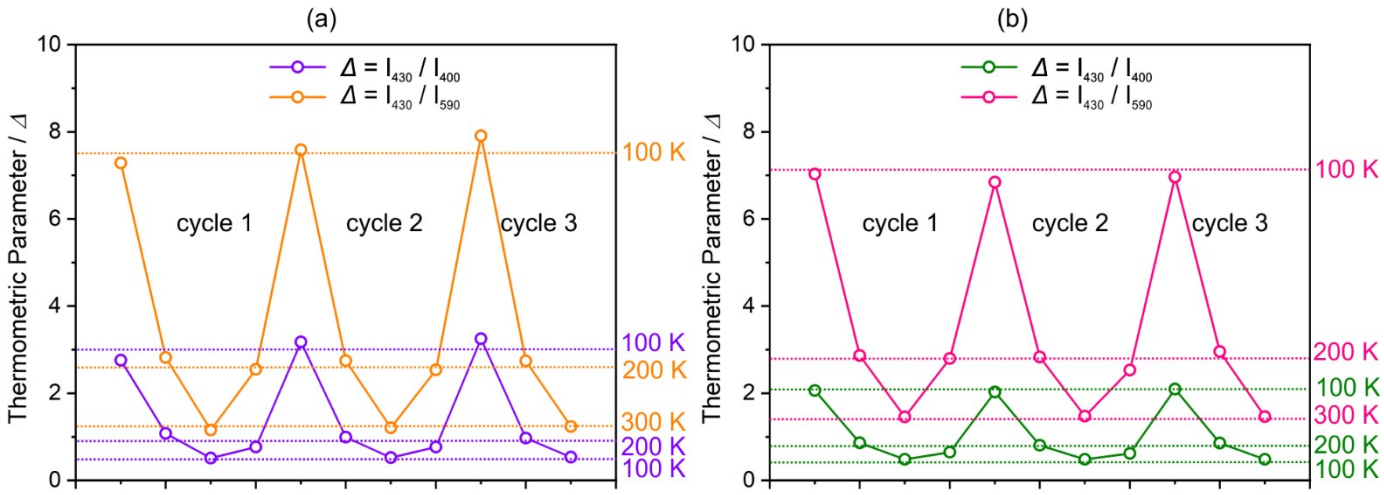

Figure S20. Three cycles of repeatability data of thermometric parameters I_{430}/I_{400} and I_{430}/I_{590} of **SmAu** for 275 nm (a) and 365 nm (b) excitation light. They were measured for three temperatures 100, 200, and 300 K.

References:

(1) M. Llunell, D. Casanova, J. Cirera, J. Bofill, P. Alemany, S. Alvarez, M. Pinsky and D. Avnir, *SHAPE v. 2.1. Program for the Calculation of Continuous Shape Measures of Polygonal and Polyhedral Molecular Fragments*, University of Barcelona: Barcelona, Spain, 2013

(2) D. Casanova, J. Cirera, M. Llunell, P. Alemany, D. Avnir and S. Alvarez, *J. Am. Chem. Soc.*, 2004, **126**, 1755.

(3) Y.-N. Guo, G.-F. Xu, Y. Guo and J. Tang, *Dalton Trans*., 2011, **40**, 9953–9963.

(4) K. Kumar, D. Abe, K. Komori-Orisaku, O. Stefanczyk, K. Nakabayashi, J. R. Shakirova, S. P. Tunik and S. Ohkoshi, *RSC Adv.*, 2019, **9**, 23444-23449.

(5) J. J. Le Roy, S. I. Gorelsky, I. Korobkov and M. Murugesu, *Organometallics*, 2015, **34**, 1415.

(6) J. D. Rinehart and J. R. Long, *Dalton Trans.*, 2012, **41**, 13572.

(7) S. K. Gupta, T. Rajeshkumar, G. Rajaraman and R. Murugavel, *Chem. Commun.*, 2016, **52**, 7168.

(8) J. J. Baldovi, J. M. Clemente-Juan, E. Coronado, Y. Duan, A. Gaita-Arino and C. Gimenez-Saiz, *Inorg. Chem.*, 2014, **53**, 9976.

(9) H. Wada, S. Ooka, T. Yamamura and T. Kajiwara, *Inorg. Chem.*, 2017, **56**, 147.

(10) H. Zhang, X. Wu, J. Liao, X. Kuang, W. Yang and C. Lu, *Dalton Trans.*, 2018, **47**, 1796.

(11) S. Demir, K. R. Meihaus and J. R. Long, J. *Organomet. Chem.*, 2017, **857**, 164.

(12) R. Vicente, A. Tubau, S. Speed, F. A. Mautner, F. Bierbaumer, R. C. Fischer and S.S. massoud, *New J. Chem.*, 2021, **45**, 14713.

(13) A. Arauzo, A. Lazarescu, S. Shova, E. Bartolome, R. Cases, J. Luzon, J. Bartolome and C. Turta, *Dalton Trans.*, 2014, **43**, 12342.
(14) S. Chorazy, T. Charytanowicz, J. Wang, S. Ohkoshi and B. Sieklucka, *Dalton Trans.*, 2018, **47**, 7870.
(15) A. K. Jassal, N. Aliaga-Alcalde, M. Corbella, D. Aravena, E. Ruiz and G. Hundal, *Dalton Trans.*, 2015, **44**, 15774.
(16) E. Bartolomé, A. Arauzo, J. Luzón, S. Melnic, S. Shova, D. Prodius, I. C. Nlebedim, F. Bartolomé and J. Bartolomé, *Dalton Trans.*, 2019, **48**, 15386.